0.01; Fig. 2B). No cleaved caspase-3 staining was observed in either the control or the mutant pancreases (data not shown). In the mutant pancreas, parts of the cells lining the lumens of dilated tubular structures were positively stained with Dolichos biflorus agglutinin (DBA; Fig. 2An).

Reduced Pdx1 Expression and Poor Exocrine Cell Differentiation in the Pancreases of *Rbp-j$^{f/f}$ Ptf1a.cre* Mice at E15.5

At E15.5, the Pdx1-positive pancreatic epithelium of the control mice exhibited complex and ramified networks (Fig. 3Aa,Ba). However, in *Rbp-j$^{f/f}$ Ptf1a.cre* mice, the branching of the epithelium was reduced, and dilated tubular structures remained (Fig. 3Ab). The epithelial cells, especially in the dilated tubular walls, were negative or faintly stained for Pdx1 (Fig. 3Ab,Bb). At around this stage, Hes1 expression was diffusely detected in the pancreatic mesenchyme (Fig. 3Ac,Ad). In the control epithelium, Hes1-positive cells were reduced compared with those at earlier stages, but were still present (Fig. 3Ac), and neurogenin 3 expression peaked between E13.5 and E15.5 (Figs. 2e, 3Ae). In contrast, Hes1 expression was significantly decreased in the mutant epithelium (Fig. 3Ad) and the most of the cells of the dilated tubular structures remained negative for both Hes1 (Fig. 3Ad) and neurogenin 3 (Fig. 3Af). The number of endocrine cells per section detected by synaptophysin (Fig. 3Ag,Ah), glucagon (Fig. 3Ai,Aj), and insulin (Fig. 3Ak,Al) immunostaining did not seem to change substantially. We estimated the total endocrine cell mass from the synaptophysin-positive area in multiple, evenly spaced sections taken through the pancreas. In the mutant pancreas, the endocrine cell mass decreased to 87% of that of the control (*Rbp-j$^{f/+}$ Ptf1a.cre*, 205,736 ± 7,194 vs. *Rbp-j$^{f/f}$ Ptf1a.cre*, 178,745 ± 3,954 pixels; $P = 0.02$). At this stage, amylase-positive cells were present in the acinar region of the control pancreas (Fig. 3Am), but these cells were significantly reduced in number in the mutant pancreas (Fig. 3An). Most of the cells lining the lumens of dilated tubular structures in the mutant pancreas stained positively with DBA (Fig. 3Ap), and the number of phospho-histone H3–positive proliferating cells was reduced (Fig. 3Ar compared with Fig. 3Aq). We next used immunofluorescence to further investigate the expression and localization of Pdx1, amylase, and phospho-histone H3. Pdx1 was uniformly expressed in the control pancreas, and all amylase-expressing cells also stained for Pdx1 (Fig. 3Ba,Bc,Be). However, in the mutant, Pdx1 expression was significantly reduced (Fig. 3Bb) and exocrine cell differentiation was severely impaired (Fig. 3Bd). In the control pancreas, differentiated exocrine cells exhibited active division (Fig. 3Bg). However, both exocrine cells and proliferating cells were sparsely distributed in the mutant pancreas (Fig. 3Ar,An,Bh). No cleaved caspase-3 staining was observed in both the control and the mutant pancreas (data not shown).

Small Pancreas With Increased Exocrine Cell Proliferation in *Rbp-j$^{f/f}$ Ptf1a.cre* Mice at Postnatal Day 0

At postnatal day (P) 0, total pancreatic size was obviously decreased (Fig. 4A), but islet formation was more prominent in the *Rbp-j$^{f/f}$ Ptf1a.cre* mice than in the control mice (Fig. 4Ba–Bh). Cytokeratin-positive dilated ductular structures occupied a small part of the mutant pancreas (Fig. 4Bj). The area of amylase-positive cells was significantly smaller in the mutant pancreas (Fig. 4Bl) than that in the control pancreas (Fig. 4Bk). Pdx1 expression was barely detectable in the exocrine cells of both the control and mutant pancreases at this time (Fig. 4Ca,Cb). The proliferation rate of the exocrine cells was much lower than at E13.5 in the control pancreas (Fig. 4Cc compared with Fig. 3Bg). However, the exocrine cells of the mutant pancreas showed active proliferation, as if in compensation for inadequate differentiation (Fig. 4A, Cd). The percentage of proliferating acinar cells was significantly increased compared with the control group (*Rbp-j$^{f/f}$*, 0.16 ± 0.01 vs. *Rbp-j$^{f/f}$ Ptf1a.cre*, 2.03 ± 0.15%; $P < 0.01$).

We traced the lineage of *Rbp-j*–deleted pancreatic cells, because the histological changes in the mutant pancreas were not simple or uniform. β-Galactosidase activity was observed broadly and uniformly throughout the pancreatic tissues, including endocrine, ductal, and exocrine cells, in the *Rosa26R$^{f/+}$ Rbp-j$^{f/f}$ Ptf1a.cre* mice (Supplementary Figure S1E).

Catch-Up Growth of Exocrine Tissue in the Pancreases of *Rbp-j$^{f/f}$ Ptf1a.cre* Mice During the First 3 Postnatal Weeks

Significant catch-up growth occurred during the early postnatal weeks in the exocrine tissue of the *Rbp-j$^{f/f}$*

Fig. 3. Reduced Pdx1 expression and poor exocrine cell differentiation in pancreas of *Rbp-j$^{f/f}$ Ptf1a.cre* mice at embryonic day (E) 15.5. **A:** Immunohistochemistry of Pdx1 (a,b), Hes1 (c,d), neurogenin 3 (e,f), synaptophysin (g,h), glucagon (i,j), insulin (k,l), amylase (m,n), Dolichos biflorus agglutinin (DBA; o,p), and phospho-histone H3 (q,r) in the pancreas of *Rbp-j$^{f/+}$ Ptf1a.cre* and *Rbp-j$^{f/f}$ Ptf1a.cre* mice at E15.5. Except for DBA (o,p) and phospho-histone H3 (q,r), serial sections are stained. The framed areas in i and k, or j and l indicate continuous areas of the same genotypes. In the mutant pancreas, the areas of Pdx1-positive (b), Hes1-positive (d), and neurogenin 3-positive (f) cells are limited and the acinar formation is poor. **B:** Double immunofluorescence against Pdx1 (green; a,b) and amylase (red; c,d) and their merged images (e,f), and merged images of double immunofluorescence against phospho-histone H3 (green) and amylase (red; g,h). The number of Pdx1/Amylase co-positive cells and proliferating cells are significantly decreased in the mutant pancreas. Scale bars = 50 μm in A, 100 μm in B.

Fig. 4. Small pancreas with increased exocrine cell proliferation in *Rbp-j$^{f/f}$ Ptf1a.cre* mice at postnatal day (P) 0. **A:** Macroscopic dorsal view of the X-gal stained pancreases from *Rosa26R$^{f/+}$ Rbp-j$^{f/+}$ Ptf1a.cre* mice (left) and *Rosa26R$^{f/+}$ Rbp-j$^{f/f}$ Ptf1a.cre* mice (right) at P0. **B:** Immunohistochemical studies with antibodies to insulin (a,b), glucagon (c,d), somatostatin (e,f), pancreatic polypeptide (g,h), cytokeratin (i,j), and amylase (k,l) using serial pancreatic sections from *Rbp-j$^{f/+}$ Ptf1a.cre* and *Rbp-j$^{f/f}$ Ptf1a.cre* mice at P0. Islet formation is more prominent in the mutant pancreas. **C:** Merged images of double immunofluorescences against Pdx1 (green) and amylase (red) (a,b) or phospho-histone H3 (green) and amylase (red; c,d). The proportion of proliferating amylase-positive cells is 13-fold higher in the mutant. Scale bars = 100 μm.

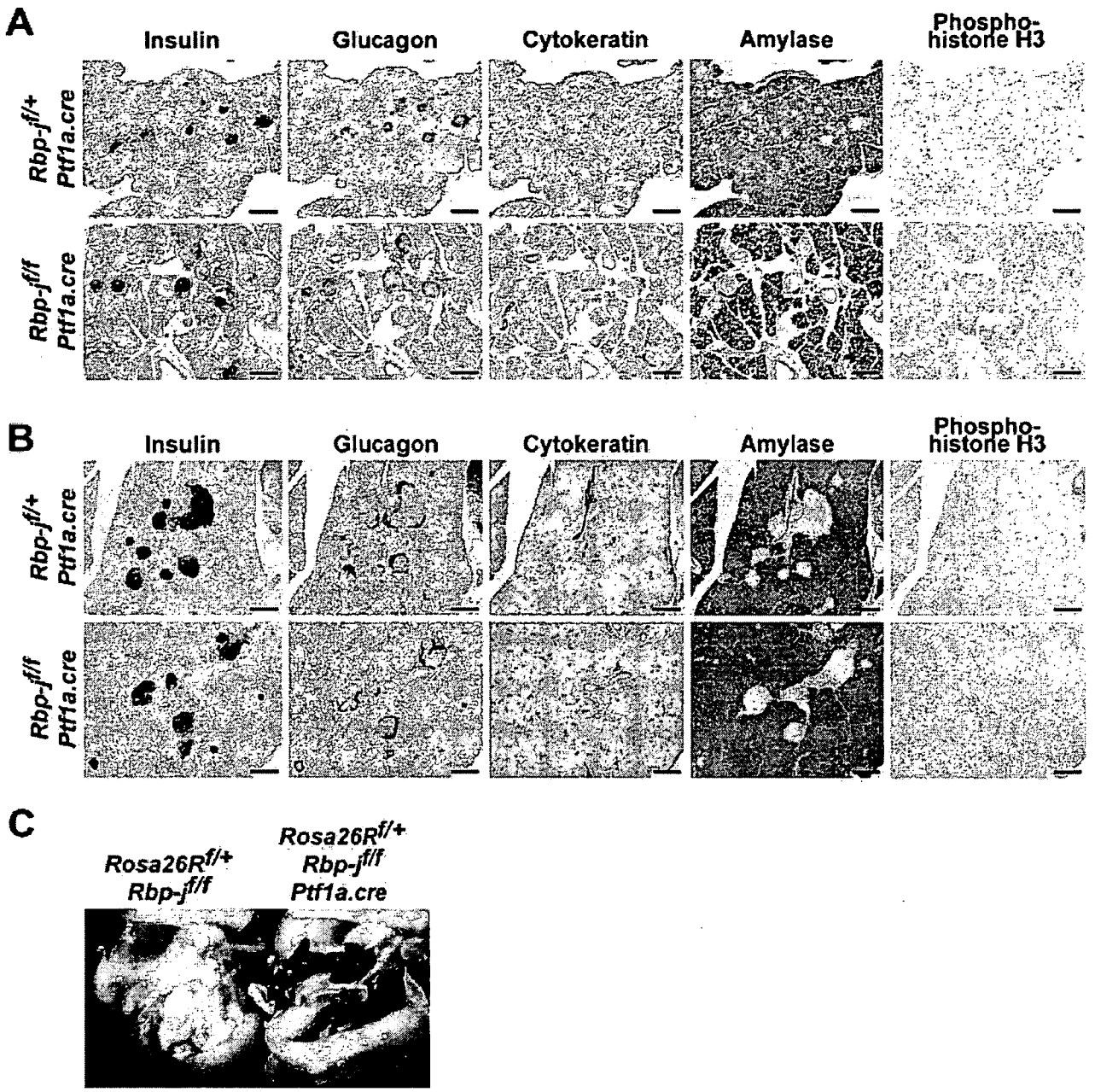

Fig. 5. By postnatal day (P) 21, Rbp-j-deficient acinar tissue showed apparently normal morphology indistinguishable from control. **A,B:** Immunohistochemical studies with antibodies to insulin, glucagon, cytokeratin, amylase, and phospho-histone H3 using serial pancreatic sections from *Rbp-j$^{f/+}$ Ptf1a.cre* and *Rbp-j$^{f/f}$ Ptf1a.cre* mice at P14 (A), and at P21 (B). **C:** X-gal staining of pancreatic regions from *Rosa26R$^{f/+}$ Rbp-j$^{f/f}$* mice (left) and *Rosa26R$^{f/+}$ Rbp-j$^{f/f}$ Ptf1a.cre* mice (right) at P21. Scale bars = 200 μm.

Ptf1a.cre mice. At postnatal day 14, amylase-positive cells were distributed patchily in the mutant compared with those in the control (Fig. 5A). However, at postnatal day 21, the mutant pancreas showed apparently normal histology and morphology, indistinguishable from that of the control pancreas (Fig. 5B,C).

Normal Pancreas, Except for Small Ductal Remnants, in Adult *Rbp-j$^{f/f}$ Ptf1a.cre* Mice

The adult *Rbp-j$^{f/f}$ Ptf1a.cre* mice had overtly normal pancreases (Fig. 6A). No mosaic pattern of recombination was apparent by X-gal staining of pancreatic sections (Fig. 6B). The deletion efficiency was assessed by Southern blot analysis of *Sph*I-digested genomic DNA prepared from adult pancreatic tissues (Fig. 6C). Only the unrecombined floxed allele was detected in the 1.2-kb band from the tail tissue, and the recombined null allele was detected in the 3-kb band from the pancreas and the pool of islets. We found

almost complete and ubiquitous recombination of the floxed allele in the adult pancreases of the *Rbp-j$^{f/f}$ Ptf1a.cre* mice. The ratio of pancreatic weight to total body weight (*Rbp-j$^{f/f}$*, 0.90 ± 0.09 vs. *Rbp-j$^{f/f}$ Ptf1a.cre*, 0.71 ± 0.10%; $P = 0.28$; Fig. 6D) was not altered in the mutants compared with that of their control littermates. The endocrine cell mass was quantified by estimating the hormone-positive area per total pancreatic area in multiple pancreatic sections. The relative cell areas of the β and α cell were not significantly altered in the *Rbp-j$^{f/f}$ Ptf1a.cre* mice (relative β cell area: *Rbp-j$^{f/f}$*, 1.24 ± 0.25 vs. *Rbp-j$^{f/f}$ Ptf1a.cre*, 1.31 ± 0.30%; $P = 0.85$; relative α cell area: *Rbp-j$^{f/f}$*, 0.19 ± 0.03 mg/dl vs. *Rbp-j$^{f/f}$ Ptf1a.cre*, 0.26 ± 0.04%; $P = 0.20$; Fig. 6E). Hematoxylin-eosin staining and immunohistochemical studies with antibodies directed against glucagon, insulin, Pdx1, somatostatin, pancreatic polypeptide, cytokeratin, and amylase revealed no abnormalities in the islet structures (Fig. 6F). In our previously reported *Rbp-j$^{f/f}$ Pdx.cre* mice, the pancreas showed striking changes in the pancreatic cell composition of the adult. Cytokeratin-positive ductal cells were abundantly present, whereas there were noticeable cystic ductal dilations (Fig. 7A, middle panels). However, in the *Rbp-j$^{f/f}$ Ptf1a.cre* mice at the same age, we observed only a focal area of ductal structures at the tip of the pancreas (Fig. 7A, lower panels). We confirmed by lineage tracing that all of these ductal and ductular structures were also derived from Rbp-j–deficient cells (Fig. 7B, blue staining).

No Signs of Endocrine or Exocrine Pancreatic Insufficiency in *Rbp-j$^{f/f}$ Ptf1a.cre* Mice

Rbp-j$^{f/f}$ Ptf1a.cre mice had normal body weights (*Rbp-j$^{f/f}$*, 27.9 ± 1.6 g vs. *Rbp-j$^{f/f}$ Ptf1a.cre*, 30.2 ± 1.5 g; $P = 0.35$; Fig. 8A). No significant differences were detected in the levels of blood glucose (*Rbp-j$^{f/f}$*, 117 ± 8 mg/dl vs. *Rbp-j$^{f/f}$ Ptf1a.cre*, 119 ± 3 mg/dl; $P = 0.76$; Fig. 8B) or plasma insulin (*Rbp-j$^{f/f}$*, 2.08 ± 0.34 ng/ml vs. *Rbp-j$^{f/f}$ Ptf1a.cre*, 2.07 ± 0.40 ng/ml; $P = 0.99$; Fig. 8C) in the fed animals. During intraperitoneal glucose tolerance testing (2 g/kg body weight), the *Rbp-j$^{f/f}$ Ptf1a.cre* mice cleared excess blood glucose at a rate similar to that of the *Rbp-j$^{f/f}$* mice (Fig. 8D). Serum amylase levels were not significantly altered in the *Rbp-j$^{f/f}$ Ptf1a.cre* mice compared with the control *Rbp-j$^{f/f}$* mice (*Rbp-j$^{f/f}$*, 1,214 ± 26 U/dl vs. *Rbp-j$^{f/f}$ Ptf1a.cre*, 1,291 ± 102 U/dl; $P = 0.41$; Fig. 8E).

DISCUSSION

Using stage-specific conditional gene targeting, we documented the effects of Rbp-j–mediated Notch signaling on pancreatic development and function. We recently reported the generation of two types of conditional Rbp-j knockout mice (Fujikura et al., 2006). *Rbp-j$^{f/f}$ Pdx.cre* mice, in which *Rbp-j* was inactivated using a *Pdx.cre* transgene, exhibited insulin-deficient diabetes with small pancreases, few islets, and lower insulin content. Pancreatic hypoplasia was caused by the premature depletion of progenitor cells and the precocious differentiation of endocrine and ductal cells. *Rbp-j$^{f/f}$ Rip.cre* mice, in which the Rbp-j gene was inactivated using a *Rip.cre* transgene, showed normal function and proliferation of the pancreatic β cells. To further assess the effects of Rbp-j–mediated Notch signaling on pancreatic development, we disrupted Rbp-j with Cre recombinase under the control of the endogenous Ptf1a promoter. We used recombination at the *Rosa26R* allele as a surrogate marker for the recombination-induced deletion of Rbp-j, because there are no established methods for the histological detection of Rbp-j. It is reasonable to assume that the difference in onset of X-gal staining between *Ptf1a.cre* and *Pdx.cre* driver lines reflects the onset of gene expression between *Ptf1a* and *Pdx1* (Guz et al., 1995; Offield et al., 1996; Edlund, 2002; Li and Edlund, 2002). Therefore, we consider that the timing of the Rbp-j deletion in pancreas development in *Rbp-j$^{f/f}$ Ptf1a.cre* mice is approximately 1 day later than in *Rbp-j$^{f/f}$ Pdx.cre* mice. However, specific and sensitive methods to directly detect and quantify Rbp-j protein in situ would be needed to confirm our results, because recombination at a *Rosa26* allele does not always guarantee deletion of the floxed *Rbp-j* loci. The difference in timing critically influenced the phenotypes of the conditional Rbp-j knockout mice, because *Rbp-j$^{f/f}$ Ptf1a.cre* mice had minimal signs of premature endocrine and ductal differentiation and showed sufficient pancreatic functions at adult ages. These results narrow the time window when Notch/Rbp-j signaling plays a critical role in the development and homeostasis of the pancreas.

In the pancreatic buds from both *Rbp-j$^{f/f}$ Pdx.cre* mice and *Rbp-j$^{f/f}$ Ptf1a.cre* mice, not all the cells lost Hes1 expression with the loss of Rbp-j. This observation suggests that the pancreatic buds contain different classes of progenitors with respect to their sensitivity to Rbp-j–mediated Notch signaling and that some other factors are also involved in maintaining Hes1 expression in the epithelium. Recently, Sox9 was shown to be one of such factors (Seymour et al., 2007).

The forced expression of the constitutively active form of the Notch1 receptor (Notch1 ICD) in the early pancreatic progenitors traps them in an undifferentiated state (Hald et al., 2003; Esni et al., 2004). Using tamoxifen-inducible expression of Notch1 ICD in mice, Murtaugh et al. also demonstrated that Pdx1-positive progenitors are sensitive to Notch signaling, even if Notch activation occurs long after the pancreas has been specified (Murtaugh et al., 2003). Fundamentally, *Rbp-j$^{f/f}$ Pdx.cre* mice have the reverse phenotype, with premature endocrine and ductal differentiation (Fujikura et al., 2006). However, our study indicates that it is in the very early stages of development that Notch signaling plays a critical role for the pancreas. This difference might have arisen from the different experimental conditions used. One study used gene disruption (loss-of-function) and the other used overexpression (gain-of-function) experiments. Alternatively, it may have been caused by differences in the modes of actions of Rbp-j and the Notch ICD.

We detected defective branching morphogenesis in both *Rbp-j$^{f/f}$ Pdx.cre* and *Rbp-j$^{f/f}$ Ptf1a.cre* mice at around E13.5. Branching morphogenesis, defined as the growth and branching of epithelial tubules during embryogenesis, is a fundamental feature of renal,

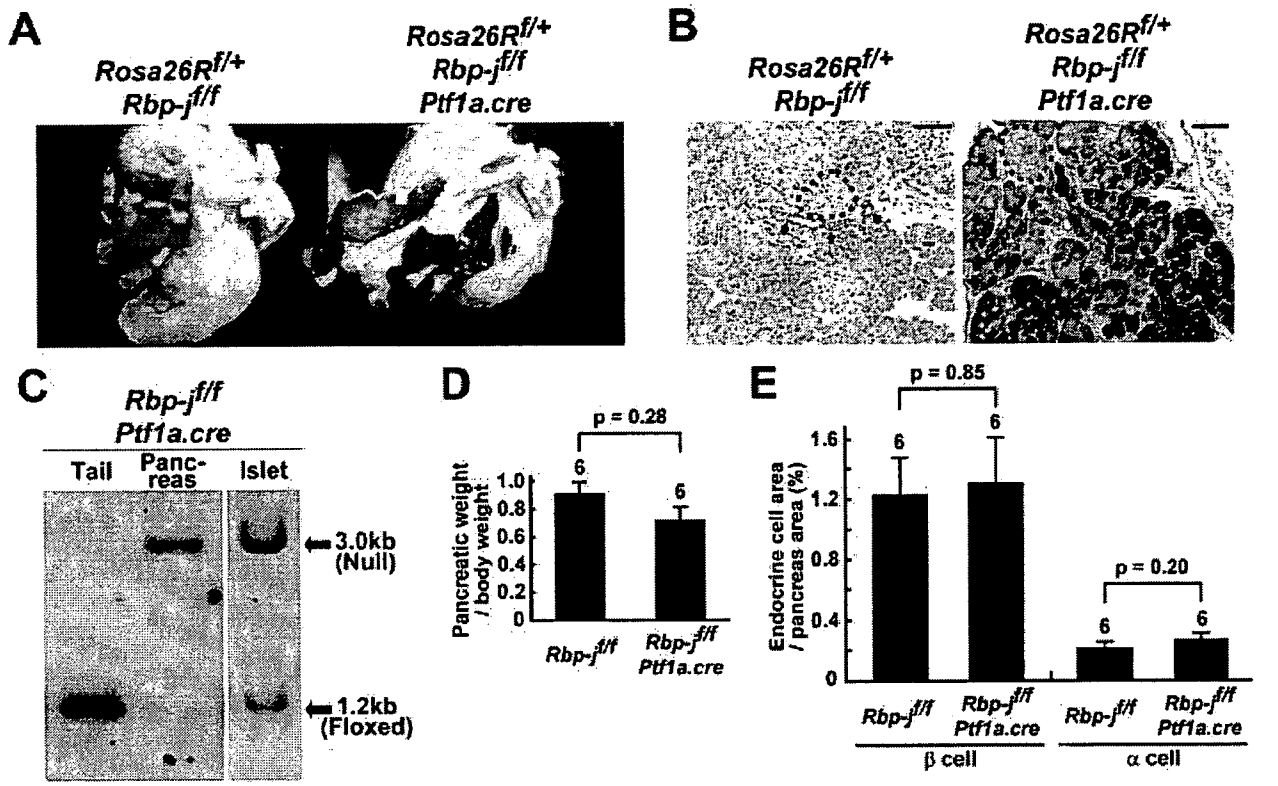

Fig. 6.

lung, mammary gland, submandibular gland, and pancreatic morphogenesis in mammals. In embryos, the pancreatic branching structures contain undifferentiated precursor cells, which migrate away to generate islet and acinar cells (Pictet and Rutter, 1972; Teitelman et al., 1993). A series of studies revealed that, apart from its well-documented involvement in cell fate decisions, Notch signaling could affect cellular proliferation (Deftos et al., 1998; Shelly et al., 1999; Satoh et al., 2004). During prostate develop-

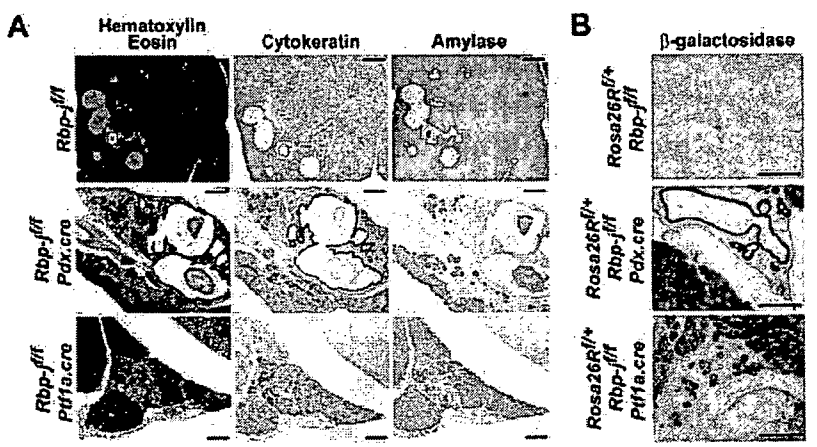

Fig. 7.

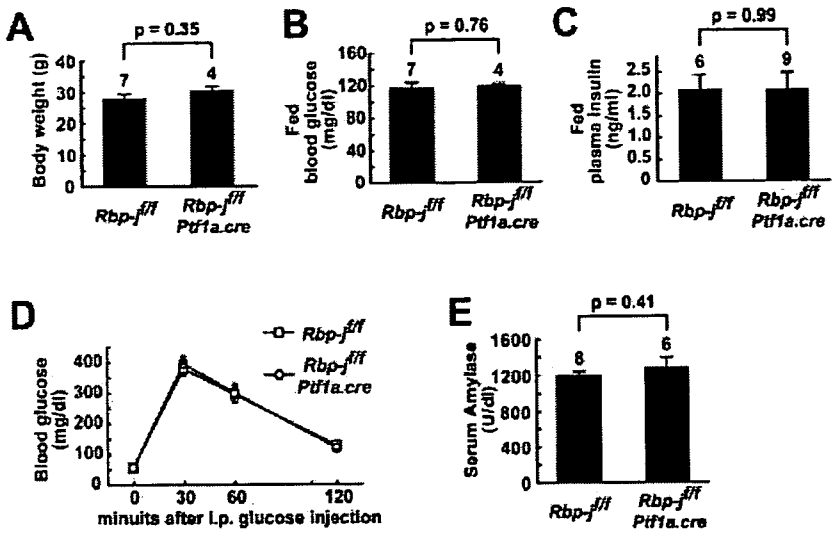

Fig. 8. No signs of endocrine or exocrine pancreatic insufficiency in *Rbp-j$^{f/f}$ Ptf1a.cre*mice. **A,B:** Body weight (A) and morning-fed blood glucose concentrations (B) of male *Rbp-j$^{f/f}$ Ptf1a.cre*mice and control littermates at 13 weeks of age. **C:** Morning-fed plasma insulin concentrations of male *Rbp-j$^{f/f}$ Ptf1a.cre*mice and control littermates at 15 weeks of age. **D:** Glucose challenge of male *Rbp-j$^{f/f}$ Ptf1a.cre*mice and control littermates at 14 weeks of age. Blood glucose levels are shown at indicated times after intraperitoneal (i.p.) glucose injections (2 g/kg body weight). There were no significant differences ($P > 0.05$) between *Rbp-j$^{f/f}$ Ptf1a.cre*mice and control mice at any given time. **E:** Amylase activity measured in serum from male *Rbp-j$^{f/f}$ Ptf1a.cre*mice and control littermates at 15 weeks of age. Standard errors and the number of mice examined are indicated on the average bars. Levels of significance (Student's *t*-tests) are shown.

ment, Notch1-expressing cells defined the progenitor cells in the prostatic epithelial cell lineage, and ablation of Notch signaling in those cells inhibits the branching morphogenesis, growth, and differentiation (Wang et al., 2004). In the pancreas, disturbed branching morphogenesis also occurs in mice deficient in *Fgf10* or its high-affinity receptor *Fgfr2-IIIb* (Bhushan et al., 2001; Pulkkinen et al., 2003). Furthermore, the overexpression of *Fgf10* in the pancreatic epithelium causes increased proliferation and the persistent upregulation of Notch components in the epithelium (Norgaard et al., 2003; Hart et al., 2003). It has recently been reported that Hes1 promotes epithelial cell proliferation by repressing the expression of the cyclin-dependent kinase inhibitor p57Kip2 during the early stages of pancreatic development (Georgia et al., 2006). Taking these data together, we consider that active Rbp-j–mediated Notch signaling cell-autonomously helps to maintain a pool of epithelial progenitors due, at least in part, to a Hes1-mediated pathway.

Both Hes1 and Pdx1 are expressed in the initial stage of exocrine cell differentiation (Esni et al., 2004). In *Rbp-j$^{f/f}$ Ptf1a.cre* mice, the lack of Rbp-j results in the reduction of both Hes1 and Pdx1 protein expression, accompanied by a decrease in acinar cell differentiation at E15.5. Hale et al. showed that the depletion of Pdx1 at E12.5 prevents the expression of Ptf1a and halts epithelial differentiation just before the formation of acini (Hale et al., 2005). Ptf1a stimulates the transcription of exocrine-specific genes and regulates the formation of pancreatic acinar cells (Krapp et al., 1998. Kawaguchi et al., 2002). The loss of Rbp-j itself might directly lead to a decrease in the transcriptional activity of Ptf1a, because Rbp-j binds Ptf1a and further stimulates its transcriptional activity (Obata et al., 2001). The disturbed pancreatic exocrine differentiation is also reminiscent of mice lacking Hes1. Mice lacking Hes1 display morphologically immature acinar cells with fewer secretory granules than are observed in the control (Jensen et al., 2000). Hes1 represses Ptf1a expression early in foregut development and define the normal boundaries of the pancreatic domain (Fukuda et al., 2006). However, the precise role of Notch/Rbp-j/Hes1 signaling during mid-pancreatic development has been unknown. Our observations indicate that, after pancreatic commitment has been induced by Ptf1a, Rbp-j supports the expression of both Hes1 and Pdx1 and facilitates the differentiation of acinar cells.

The catch-up growth of pancreatic exocrine cells has been observed not only in our pancreatic Rbp-j–deficient mice, but also in Hes1-deficient mice (Jensen et al., 2000; Fujikura et al., 2006). Stimulation of Notch signaling has been reported to diminish the pro-

Fig. 6. Normal endocrine tissue in pancreas of adult *Rbp-j$^{f/f}$ Ptf1a.cre* mice. **A:** X-gal staining of pancreatic regions from *Rosa26R$^{+/+}$ Rbp-j$^{f/f}$* mice (left) and *Rosa26R$^{+/+}$ Rbp-j$^{f/f}$ Ptf1a.cre* mice (right) at the adult stage. The mutant adult mice have overtly normal pancreases. **B:** X-gal staining of pancreatic sections from *Rosa26R$^{+/+}$ Rbp-j$^{f/f}$* mice (left) and *Rosa26R$^{+/+}$ Rbp-j$^{f/f}$ Ptf1a.cre* mice (right) at adult. Islets are encircled by dotted lines, and ducts are indicated by arrows. No mosaic pattern of recombination was seen. **C:** Pancreatic deletion of *Rbp-j* by *Ptf1a.cre*. Genomic DNA from the tail, the pancreas, and the pool of islets of *Rbp-j$^{f/f}$ Ptf1a.cre* mice were digested with *Sph*I and hybridized with the probe. **D:** The ratio of pancreatic weight to body weights of male *Rbp-j$^{f/f}$ Ptf1a.cre* mice and control littermates at 16 weeks of age. Standard errors and number of mice examined are indicated on the average bars. **E:** The β and α cell masses were determined from anti-insulin– and anti-glucagon–stained multiple sections as described in the Experimental Procedures section. Standard errors and the number of mice examined are indicated on the average bars. **F:** Immunohistochemical studies with antibodies to Pdx1, insulin, glucagon, somatostatin, and pancreatic polypeptide using serial pancreatic sections from *Rbp-j$^{f/f}$ Ptf1a.cre* mice and control littermates at 16 weeks of age. No significant changes of pancreatic cell composition are observed. Scale bars = 50 μm in A,B, 200 μm in C–F.

Fig. 7. Small ductal remnants in pancreas of adult *Rbp-j$^{f/f}$ Ptf1a.cre*mice. **A:** Hematoxylin–eosin staining, immunohistochemical studies with cytokeratin and amylase of serial pancreatic sections from *Rbp-j$^{f/f}$*, *Rbp-j$^{f/f}$ Pdx.cre*, and *Rbp-j$^{f/f}$ Ptf1a.cre*mice at 20 weeks of age. *Rbp-j$^{f/f}$ Pdx.cre* pancreas exhibits cystic ductal dilations, whereas *Rbp-j$^{f/f}$ Ptf1a.cre* pancreas show only a focal area of ductal structures at the tip. **B:** X-gal staining of pancreatic sections from *Rosa26R$^{+/+}$ Rbp-j$^{f/f}$*, *Rosa26R$^{+/+}$ Rbp-j$^{f/f}$ Pdx.cre*, and *Rosa26R$^{+/+}$ Rbp-j$^{f/f}$ Ptf1a.cre* mice (right) at adult stage. Scale bars = 200 μm.

liferation of cultured exocrine cells in a manner independent of Hes1, but related to Hey1, Hey2, and p21Cip1 (Rooman et al., 2006). However, the mechanisms of exocrine cell proliferation, especially in the growing pancreas during the perinatal period, require further investigation.

After this catch-up growth, the architecture and function of the acinar tissues of the mutant mice were almost normal. Normal adult acinar cells express little or no detectable levels of either Pdx1 or Notch pathway components (Wu et al., 1997; Miyamoto et al., 2003). Forced expression of Pdx1 in acinar cells causes a marked dysmorphogenesis and metaplasia of the exocrine pancreas (Heller et al., 2001; Miyatsuka et al., 2006). The ectopic activation of the Notch pathway has also been observed in animal models of acinar cell metaplasia and in human pancreatic cancer (Miyamoto et al., 2003). Reduced Pdx1 expression and silent Rbp-j–mediated Notch signaling in our mutant mice is compatible with the proposition that the down-regulation of Pdx1 and Notch signaling is required for the proper maintenance of the exocrine cell phenotype. Another recent study has shown that, in adult acinar cells, Ptf1a protein associates exclusively with Rbp-L, a paralog of Rbp-j, and that the Ptf1a/Rbp-L complex stimulates the promoter activities of acinar-specific genes more effectively than does the Ptf1a/Rbp-j complex (Beres et al., 2006). The findings of our studies indicate that Rbp-j–mediated Notch signaling is not essential for the function of mature acinar cells after they have fully differentiated.

Focal areas of ductal differentiation and more widespread areas of ductal structures with prominent cystic changes were detected in *Rbp-j$^{f/f}$ Ptf1a.cre* and *Rbp-j$^{f/f}$ Pdx.cre* mice, respectively. Like *Rbp-j$^{f/f}$ Pdx.cre* mice, mice with hypomorphic Pdx1 alleles develop a pancreatic ductal cyst lined with a simple cuboidal epithelium, which is positive for cytokeratin but negative for Nkx6.1, a β cell differentiation marker (Fujitani et al., 2006). The inhibition of branching morphogenesis by the depletion of Pdx1 has been correlated with decreased acinar cell formation, and the residual cells adopt the phenotype of ductal cells (Hale et al., 2005). These results indicate that Rbp-j blocks the transition from pancreatic progenitor epithelium to ductal epithelium by maintaining the expression level of Pdx1. Among the Notch receptors, Notch2 is strongly expressed in the pancreatic ductal cells from the embryo to the adult (Lammert et al., 2000, and our unpublished data). We have also generated pancreas-specific *Notch2* knockout mice. However, we have detected no differences between the control and the knockout mice (unpublished data). The physiological significance of the expression of the Notch receptor in pancreatic ductal cells requires further investigation.

All our stage-specific knockout mice generated using the *Pdx1*, *Ptf1a*, and *insulin 2* promoters suggest that Rbp-j–mediated Notch signaling is essential for the expansion of early pancreatic progenitors by maintaining the expression of both Hes1 and Pdx1, but is not essential for mature pancreatic cell functions.

EXPERIMENTAL PROCEDURES

Generation of Pancreas-Specific Rbp-j Knockout Mice

The generation of mice bearing a floxed allele of *Rbp-j* was described previously (Han et al., 2002). *Ptf1a.cre* mice in which the Cre recombinase gene was knocked-in into the *Ptf1a* gene locus were reported previously (Kawaguchi et al., 2002). Mice homozygous for the floxed *Rbp-j* allele (*Rbp-j$^{f/f}$*) were crossed with *Ptf1a.cre* mice. The double heterozygous mice were then crossed with *Rbp-j$^{f/+}$* mice, resulting in *Rbp-j$^{f/f}$ Ptf1a.cre* mice and their control littermates. Genotyping and assessment of deletion efficiency were performed by Southern blot analyses on genomic DNA obtained from tails, pancreases, and pool of islets. Other pancreas-specific Rbp-j knockout mice by using *Pdx.cre* transgenic mice were recently reported (Gu et al., 2002; Fujikura et al., 2006). *Rosa26-lacZ* reporter mice were purchased from The Jackson Laboratory (Bar Harbor, ME; Soriano, 1999).

X-gal Staining

For visualization of *Pdx.cre*- or *Ptf1a.cre*-mediated loxP recombination, mice heterozygous for floxed *Rbp-j* and homozygous for *Rosa26R* alleles, *Rosa26R$^{f/f}$ Rbp-j$^{f/+}$*, were crossed with double heterozygous *Rbp-j$^{f/+}$ Pdx.cre* or *Rbp-j$^{f/+}$ Ptf1a.cre* mice. Genotyping of floxed *Rosa26R* alleles was performed by DNA dot blot analyses on genomic DNA obtained from tails or yolk sacs. A 1.2-kb *Cla*I–*Sac*I LacZ fragment was used as a probe to detect the floxed *Rosa26R* allele. Whole embryos or pancreatic regions were fixed with 4% paraformaldehyde in phosphate-buffered saline (PBS) for 1 hr at 4°C and washed with PBS. To prepare cryostat sections, pancreases were dissected, fixed in 4% paraformaldehyde in PBS for 1 hr at 4°C, and frozen in OCT compound (Sakura, Tokyo, Japan). Ten-micrometer sections were cut, air-dried for 30 min, and then post-fixed for 5 min in 4% paraformaldehyde. Fixed embryos, pancreatic regions, or tissue sections were incubated at 30°C in a solution containing PBS, potassium ferricyanide, potassium ferrocyanide, $MgCl_2$, and galactopyranoside dissolved in dimethyl sulfoxide. After staining with X-gal, E9.5 and E10.5 embryos were dehydrated in methanol and cleared in a 2:1 solution of benzyl benzoate:benzyl alcohol. Macroscopic pictures were taken using an Axioskop Microscope (Carl Zeiss, Jena, Germany). X-gal–positive cells were identified by their blue staining.

Immunohistochemical Analyses

Embryos or isolated pancreases were fixed with 4% paraformaldehyde in PBS for overnight at 4°C, then paraffin embedded, and 5-μm sections were cut and mounted on glass slides. Slides were de-waxed and rehydrated. Except for the detection of hormones, the mounted sections were subjected to antigen retrieval by autoclaving at 121°C for 5 min with 10 mM citrate buffer. Endogenous peroxidase was inactivated with 0.3% H_2O_2 in methanol for 30 min. The slides were blocked for 1 hr at room temperature with a reagent containing casein (DAKO Protein Block Serum-Free So-

lution; Dako, Glostrup, Denmark), then stained overnight at 4°C with the following primary antibodies (Abs) or lectin: guinea pig anti-insulin antibody, 1:500 dilution (Dako); rabbit anti-glucagon antibody, 1:500 dilution (Dako); rabbit anti-somatostatin antibody, 1:500 dilution (Dako); rabbit anti-pancreatic polypeptide antibody, 1:500 dilution (Dako); rabbit anti–pan-cytokeratin antibody, 1:200 dilution (Santa Cruz, Santa Cruz, CA); rabbit anti-amylase antibody, 1:1,000 dilution (Sigma-Aldrich, St. Louis, MO); goat anti-amylase antibody, 1:50 dilution (Santa Cruz); rabbit anti-carboxypeptidase A antibody, 1:750 dilution (BioTrend, Cologne, Germany); rabbit anti-Pdx1 antibody, 1:5,000 dilution (Peshavaria et al., 1994); mouse anti-neurogenin 3 antibody, 1:100 dilution (Developmental Studies Hybridoma Bank, Iowa, IA); rabbit anti-Hes1 antibody, 1:10,000 dilution (gift from Dr. R. Kageyama); rabbit anti-synaptophysin antibody, 1:50 dilution (Dako); rabbit anti–phospho-histone H3 antibody, 1:50 dilution (Cell Signaling Technology, Beverly, MA); rabbit anti-cleaved caspase-3 antibody, 1:100 dilution (Cell Signaling Technology); rabbit anti–Rbp-L antibody, 1:200 dilution (gift from Dr. R. MacDonald); and biotinylated DBA (Vector, Burlingame, CA). The slides were washed with PBS the following day and incubated for 1 hr at room temperature with the following secondary antibodies: biotinylated goat anti-guinea pig IgG antibody, 1:200 dilution; biotinylated goat anti-rabbit IgG antibody, 1:200 dilution; biotinylated horse anti-mouse IgG antibody (all from Vector). The slides were then incubated with avidin–biotin complex (ABC) reagent (Vectastain Elite ABC Kit; Vector) for 50 min at room temperature followed by the addition of diaminobenzidine tetrahydrochloride (Dako) as a substrate–chromogen solution. After hematoxylin counterstaining and dehydration, slides were mounted in mounting medium (MGK-S; Matsunami, Osaka, Japan) and pictures were taken using an Axioskop Microscope (Carl Zeiss).

For immunofluorescence, Alexa488 donkey anti-rabbit IgG antibody, 1:200 dilution, and Alexa546 donkey anti-goat IgG antibody, 1:200 dilution (both from Molecular Probes, Eugene, OR), were used as secondary antibodies. Images were captured using a Zeiss LSM 5 PASCAL confocal microscope (Carl Zeiss).

Quantitative Morphometry and Cell Counting

The relative numbers of Hes1, neurogenin 3, synaptophysin, and phosphohistone H3–positive cells to Pdx1-positive cells were calculated from the average of counts of 1,635 cells at E13.5 from each mouse. Four to six mice were examined for each group. The endocrine cell mass at E15.5 was calculated from the total area (pixel number) of synaptophysin-positive cells. The area of synaptophysin-positive neuronal fibers was excluded. Four mice were used for each group, and 4 to 11 sections were examined for each mouse. The acinar cell proliferation rate at P0 was determined by the ratio of the number of amylase/phospho-histone H3 double-positive cells to the total number of amylase-positive cells. For each group, four mice were used. An average of 19,000 cells were counted per mouse. The endocrine cell mass at 16 weeks of age was calculated as the ratio of each hormone-positive cell area to the total area of the pancreas section using an image analysis program (Scion Image; Scion, Frederick, MD). For each group, six mice were used. The measurement and calculation were done with a total of 18 sections that had been prepared from the six pancreases (three sections per mouse). The three sections from each mouse were far apart from one another. The whole area of each section was investigated, and the percentage of insulin- or glucagon-positive cell area relative to the whole pancreatic area was determined. All values are expressed as mean ± standard error. The statistical significance was tested with Student's *t*-test or Welch's *t*-test.

Analysis of Metabolic Parameters

Blood glucose values were determined from whole venous blood taken from mouse tails using an automatic glucometer (Glutest Ace; Sanwa Kagaku, Aichi, Japan). Blood samples for insulin and amylase measurements were taken from retro-orbital venous plexuses. Plasma insulin levels were measured using an enzyme-linked immunosorbent assay kit (Morinaga, Kanagawa, Japan). Amylase activity was measured according to the Caraway method using a kit (Amylase-Test Wako; Wako, Osaka, Japan). All values are expressed as mean ± standard error. The statistical significance was tested with Student's *t*-test.

Glucose Tolerance Test

After an overnight fast, the mice were injected intraperitoneally with glucose at 2.0 g/kg body weight. Blood samples were taken at various time points and blood glucose concentration was measured with an automatic glucometer (Glutest Ace; Sanwa Kagaku). All values are expressed as mean ± standard error. The statistical significance was tested with Student's *t*-test.

ACKNOWLEDGMENTS

We thank Prof. Douglas A. Melton for providing *Pdx.cre* mice, Prof. Christopher V. E. Wright for *Ptf1a.cre* mice and Pdx1 antibody, Prof. Ryoichiro Kageyama for Hes1 antibody, and Prof. Raymond MacDonald for Rbp-L antibody. We also thank Prof. Tasuku Honjo for his encouragement throughout this project.

REFERENCES

Apelqvist A, Li H, Sommer L, Beatus P, Anderson DJ, Honjo T, Hrabe de Angelis M, Lendahl U, Edlund H. 1999. Notch signalling controls pancreatic cell differentiation. Nature 400:877–881.

Beres TM, Masui T, Swift GH, Shi L, Henke RM, MacDonald RJ. 2006. PTF1 is an organ-specific and Notch-independent basic helix-loop-helix complex containing the mammalian Suppressor of Hairless (RBP-J) or its paralogue, RBP-L. Mol Cell Biol 26:117–130.

Bhushan A, Itoh N, Kato S, Thiery JP, Czernichow P, Bellusci S, Scharfmann R. 2001. Fgf10 is essential for maintaining the proliferative capacity of epithelial progenitor cells during early pancreatic organogenesis. Development 128:5109–5117.

Buono KD, Robinson GW, Martin C, Shi S, Stanley P, Tanigaki K, Honjo T, Hennighausen L. 2006. The canonical Notch/RBP-J signaling pathway controls the balance of cell lineages in mammary epithelium during pregnancy. Dev Biol 293: 565–580.

Cockell M, Stevenson BJ, Strubin M, Hagenbuchle O, Wellauer PK. 1989. Identification of a cell-specific DNA-binding activity that interacts with a transcriptional activator of genes expressed in the acinar pancreas. Mol Cell Biol 9:2464–2476.

Deftos ML, He YW, Ojala EW, Bevan MJ. 1998. Correlating notch signaling with thymocyte maturation. Immunity 9:777–786.

Edlund H. 2002. Pancreatic organogenesis—developmental mechanisms and implications for therapy. Nat Rev Genet 3:524–532.

Esni F, Ghosh B, Biankin AV, Lin JW, Albert MA, Yu X, MacDonald RJ, Civin CI, Real FX, Pack MA, Ball DW, Leach SD. 2004. Notch inhibits Ptf1 function and acinar cell differentiation in developing mouse and zebrafish pancreas. Development 131:4213–4224.

Fujikura J, Hosoda K, Iwakura H, Tomita T, Noguchi M, Masuzaki H, Tanigaki K, Yabe D, Honjo T, Nakao K. 2006. Notch/Rbp-j signaling prevents premature endocrine and ductal cell differentiation in the pancreas. Cell Metab 3:59–65.

Fujitani Y, Fujitani S, Boyer DF, Gannon M, Kawaguch Y, Ray M, Shiota M, Stein RW, Magnuson MA, Wright CV. 2006. Targeted deletion of a cis-regulatory region reveals differential gene dosage requirements for Pdx1 in foregut organ dedifferentiation and pancreas formation. Genes Dev 20:253–266.

Fukuda A, Kawaguchi Y, Furuyama K, Kodama S, Horiguchi M, Kuhara T, Koizumi M, Boyer DF, Fujimoto K, Doi R, Kageyama R, Wright CV, Chiba T. 2006. Ectopic pancreas formation in Hes1-knockout mice reveals plasticity of endodermal progenitors of the gut, bile duct, and pancreas. J Clin Invest 116: 1484–1493.

Georgia S, Soliz R, Li M, Zhang P, Bhushan A. 2006. p57 and Hes1 coordinate cell cycle exit with self-renewal of pancreatic progenitors. Dev Biol 298:22–31.

Gittes GK, Rutter WJ. 1992. Onset of cell-specific gene expression in the developing mouse pancreas. Proc Natl Acad Sci U S A 89:1128–1132.

Gu G, Dubauskaite J, Melton DA. 2002. Direct evidence for the pancreatic lineage: NGN3+ cells are islet progenitors and are distinct from duct progenitors. Development 129:2447–2457.

Guz Y, Montminy MR, Stein R, Leonard J, Gamer LW, Wright CV, Teitelman G. 1995. Expression of murine STF-1, a putative insulin gene transcription factor, in beta cells of pancreas, duodenal epithelium and pancreatic exocrine and endocrine progenitors during ontogeny. Development 121:11–18.

Hald J, Hjorth JP, German MS, Madsen OD, Serup P, Jensen J. 2003. Activated Notch1 prevents differentiation of pancreatic acinar cells and attenuate endocrine development. Dev Biol 260:426–37.

Hale MA, Kagami H, Shi L, Holland AM, Elsasser HP, Hammer RE, MacDonald RJ. 2005. The homeodomain protein PDX1 is required at mid-pancreatic development for the formation of the exocrine pancreas. Dev Biol 286:225–237.

Hamada Y, Kadokawa Y, Okabe M, Ikawa M, Coleman JR, Tsujimoto Y. 1999. Mutation in ankyrin repeats of the mouse Notch2 gene induces early embryonic lethality. Development 126:3415–3424.

Han H, Tanigaki K, Yamamoto N, Kuroda K, Yoshimoto M, Nakahata T, Ikuta K, Honjo T. 2002. Inducible gene knockout of transcription factor recombination signal binding protein-J reveals its essential role in T versus B lineage decision. Int Immunol 14:637–645.

Hart A, Papadopoulou S, Edlund H. 2003. Fgf10 maintains notch activation, stimulates proliferation, and blocks differentiation of pancreatic epithelial cells. Dev Dyn 228:185–193.

Heller RS, Stoffers DA, Bock T, Svenstrup K, Jensen J, Horn T, Miller CP, Habener JF, Madsen OD, Serup P. 2001. Improved glucose tolerance and acinar dysmorphogenesis by targeted expression of transcription factor PDX-1 to the exocrine pancreas. Diabetes 50:1553–1561.

Heller RS, Jenny M, Collombat P, Mansouri A, Tomasetto C, Madsen OD, Mellitzer G, Gradwohl G, Serup P. 2005. Genetic determinants of pancreatic epsilon-cell development. Dev Biol 286:217–224.

Hrabé de Angelis M, McIntyre JII, Gossler A. 1997. Maintenance of somite borders in mice requires the Delta homologue Dll1. Nature 386:717–721.

Ishibashi M, Ang SL, Shiota K, Nakanishi S, Kageyama R, Guillemot F. 1995. Targeted disruption of mammalian hairy and Enhancer of split homolog-1 (HES-1) leads to up-regulation of neural helix-loop-helix factors, premature neurogenesis, and severe neural tube defects. Genes Dev 9:3136–3148.

Jensen J, Pedersen EE, Galante P, Hald J, Heller RS, Ishibashi M, Kageyama R, Guillemot F, Serup P, Madsen OD. 2000. Control of endodermal endocrine development by Hes-1. Nat Genet 24:36–44.

Kageyama R, Ohtsuka T. 1999. The Notch-Hes pathway in mammalian neural development. Cell Res 9:179–188.

Kato H, Sakai T, Tamura K, Minoguchi S, Shirayoshi Y, Hamada Y, Tsujimoto Y, Honjo T. 1996. Functional conservation of mouse Notch receptor family members. FEBS Lett 395:221–224.

Kawaguchi Y, Cooper B, Gannon M, Ray M, MacDonald RJ, Wright CV. 2002. The role of the transcriptional regulator Ptf1a in converting intestinal to pancreatic progenitors. Nat Genet 32:128–134.

Krapp A, Knofler M, Ledermann B, Burki K, Berney C, Zoerkler N, Hagenbuchle O, Wellauer PK. 1998. The bHLH protein PTF1-p48 is essential for the formation of the exocrine and the correct spatial organization of the endocrine pancreas. Genes Dev 12:3752–3763.

Lammert E, Brown J, Melton DA. 2000. Notch gene expression during pancreatic organogenesis. Mech Dev 94:199–203.

Li H, Edlund H. 2001. Persistent expression of Hlxb9 in the pancreatic epithelium impairs pancreatic development. Dev Biol 240:247–253.

Minoguchi S, Taniguchi Y, Kato H, Okazaki T, Strobl LJ, Zimber-Strobl U, Bornkamm GW, Honjo T. 1997. RBP-L, a transcription factor related to RBP-Jkappa. Mol Cell Biol 17:2679–2687.

Miyamoto Y, Maitra A, Ghosh B, Zechner U, Argani P, Iacobuzio-Donahue CA, Sriuranpong V, Iso T, Meszoely IM, Wolfe MS, Hruban RH, Ball DW, Schmid RM, Leach SD. 2003. Notch mediates TGF alpha-induced changes in epithelial differentiation during pancreatic tumorigenesis. Cancer Cell 3:565–576.

Miyatsuka T, Kaneto H, Shiraiwa T, Matsuoka TA, Yamamoto K, Kato K, Nakamura Y, Akira S, Takeda K, Kajimoto Y, Yamasaki Y, Sandgren EP, Kawaguchi Y, Wright CV, Fujitani Y. 2006. Persistent expression of PDX-1 in the pancreas causes acinar-to-ductal metaplasia through Stat3 activation. Genes Dev 20:1435–1440.

Murtaugh LC, Stanger BZ, Kwan KM, Melton DA. 2003. Notch signaling controls multiple steps of pancreatic differentiation. Proc Natl Acad Sci U S A 100: 14920–14925.

Norgaard GA, Jensen JN, Jensen J. 2003. FGF10 signaling maintains the pancreatic progenitor cell state revealing a novel role of Notch in organ development. Dev Biol 264:323–338.

Obata J, Yano M, Mimura H, Goto T, Nakayama R, Mibu Y, Oka C, Kawaichi M. 2001. p48 subunit of mouse PTF1 binds to RBP-Jkappa/CBF-1, the intracellular mediator of Notch signalling, and is expressed in the neural tube of early stage embryos. Genes Cells 6:345–360.

Offield MF, Jetton TL, Labosky PA, Ray M, Stein RW, Magnuson MA, Hogan BL, Wright CV. 1996. PDX-1 is required for pancreatic outgrowth and differentiation of the rostral duodenum. Development 122:983–995.

Oka C, Nakano T, Wakeham A, de la Pompa JL, Mori C, Sakai T, Okazaki S, Kawaichi M, Shiota K, Mak TW, Honjo T. 1995. Disruption of the mouse RBP-J kappa gene results in early embryonic death. Development 121:3291–3301.

Peshavaria M, Gamer L, Henderson E, Teitelman G, Wright CV, Stein R. 1994. XIHbox 8, an endoderm-specific Xenopus homeodomain protein, is closely related to a mammalian insulin gene transcription factor. Mol Endocrinol 8:806–816.

Pictet R, Rutter WJ. 1972. Development of the embryonic pancreas. In: Steiner DF, Frenkel N. editors. Handbook of physiology. Washington DC: American Physiology Society. p 25–66.

Pulkkinen MA, Spencer-Dene B, Dickson C, Otonkoski T. 2003. The IIIb isoform of fibroblast growth factor receptor 2 is required for proper growth and branching of pancreatic ductal epithelium but not for differentiation of exocrine or endocrine cells. Mech Dev 120:167–175.

Rooman I, De Medts N, Baeyens L, Lardon J, De Breuck S, Heimberg H, Bouwens L. 2006. Expression of the notch signaling

pathway and effect on exocrine cell proliferation in adult rat pancreas. Am J Pathol 169:1206–1214.

Satoh Y, Matsumura I, Tanaka H, Ezoe S, Sugahara H, Mizuki M, Shibayama H, Ishiko E, Ishiko J, Nakajima K, Kanakura Y.. 2004. Roles for c-Myc in self-renewal of hematopoietic stem cells. J Biol Chem 279:24986–24993.

Seymour PA, Freude KK, Tran MN, Mayes EE, Jensen J, Kist R, Scherer G, Sander M. 2007. SOX9 is required for maintenance of the pancreatic progenitor cell pool. Proc Natl Acad Sci U S A 104:1865–1870.

Shelly LL, Fuchs C, Miele L. 1999. Notch-1 inhibits apoptosis in murine erythroleukemia cells and is necessary for differentiation induced by hybrid polar compounds. J Cell Biochem 73:164–175.

Soriano P. 1999. Generalized lacZ expression with the ROSA26 reporter strain. Nat Genet 21:70–71.

Swiatek PJ, Lindsell CE, del Amo FF, Weinmaster G, Gridley T. 1994. Notch1 is essential for postimplantation development in mice. Genes Dev 15:707–719.

Tanigaki K, Han H, Yamamoto N, Tashiro K, Ikegawa M, Kuroda K, Suzuki A, Nakano T, Honjo T. 2002. Notch-RBP-J signaling is involved in cell fate determination of marginal zone B cells. Nat Immunol 3:443–450.

Tanigaki K, Tsuji M, Yamamoto N, Han H, Tsukada J, Inoue H, Kubo M, Honjo T. 2004. Regulation of alphabeta/gammadelta T cell lineage commitment and peripheral T cell responses by Notch/RBP-J signaling. Immunity 20:611–622.

Teitelman G, Alpert S, Polak JM, Martinez A, Hanahan D. 1993. Precursor cells of mouse endocrine pancreas coexpress insulin, glucagon and the neuronal proteins tyrosine hydroxylase and neuropeptide Y, but not pancreatic polypeptide. Development 118:1031–1039.

Wang XD, Shou J, Wong P, French DM, Gao WQ. 2004. Notch1-expressing cells are indispensable for prostatic branching morphogenesis during development and re-growth following castration and androgen replacement. J Biol Chem 279: 24733–24744.

Wiedenmann B, Franke WW, Kuhn C, Moll R, Gould VE. 1986. Synaptophysin: a marker protein for neuroendocrine cells and neoplasms. Proc Natl Acad Sci U S A 83:3500–3504.

Wu KL, Gannon M, Peshavaria M, Offield MF, Henderson E, Ray M, Marks A, Gamer LW, Wright CV, Stein R. 1997. Hepatocyte nuclear factor 3beta is involved in pancreatic beta-cell-specific transcription of the pdx-1 gene. Mol Cell Biol 17:6002–6013.

Xue Y, Gao X, Lindsell CE, Norton CR, Chang B, Hicks C, Gendron-Maguire M, Rand B, Weinmaster G, Gridley T. 1999. Embryonic lethality and vascular defects in mice lacking the Notch ligand Jagged1. Hum Mol Genet 8:723–730.

Yamamoto N, Tanigaki K, Han H, Hiai H, Honjo T. 2003. Notch/RBP-J signaling regulates epidermis/hair fate determination of hair follicular stem cells. Curr Biol 13:333–338.

THE JOURNAL OF BIOLOGICAL CHEMISTRY VOL. 282, NO. 40, pp. 29574–29583, October 5, 2007

Genetic and Pharmacological Inhibition of Rho-associated Kinase II Enhances Adipogenesis*

Received for publication, July 20, 2007 Published, JBC Papers in Press, August 6, 2007, DOI 10.1074/jbc.M705972200

Michio Noguchi‡, Kiminori Hosoda‡1, Junji Fujikura‡, Muneya Fujimoto‡, Hiroshi Iwakura‡, Tsutomu Tomita‡, Takako Ishii‡, Naoki Arai‡, Masakazu Hirata‡, Ken Ebihara‡, Hiroaki Masuzaki‡, Hiroshi Itoh‡, Shuh Narumiya§, and Kazuwa Nakao‡

From the ‡Department of Medicine and Clinical Science, Kyoto University Graduate School of Medicine, Kyoto 606-8507, Japan and the §Department of Pharmacology, Kyoto University Faculty of Medicine, Kyoto 606-8501, Japan

Rho-associated kinase (ROCK) regulates reorganization of actin cytoskeleton. During adipogenesis, the structure of filamentous actin is converted from long stress fibers to cortical actin, suggesting that the ROCK is involved in adipogenesis. Two ROCK isoforms have been identified: ROCK-I and ROCK-II. However, pharmacological inhibitors of ROCK cannot distinguish two ROCK isoforms. In the present study, we examined the role of ROCK in adipogenesis and actin cytoskeleton using genetic and pharmacological approaches. Y-27632, which inhibits the activity of both ROCK isoforms, enhanced adipogenesis through the up-regulation of adipogenic transcription factors in 3T3-L1 cells. Furthermore, Y-27632 restored inhibition of adipogenesis by lysophosphatidic acid, which activates Rho. Regarding actin cytoskeleton, Y-27632 disrupted stress fibers in 3T3-L1 preadipocytes. Next, we analyzed adipogenesis of mouse embryonic fibroblasts (MEFs) derived from ROCK-I and ROCK-II knock-out mice, respectively. Adipogenesis of ROCK-II (−/−) MEFs was markedly enhanced compared with wild-type MEFs while that of ROCK-I (−/−) MEFs was not. In contrast to pharmacological approaches, no obvious alteration was found in actin cytoskeleton of ROCK-II (−/−) MEFs compared with wild-type MEFs. In 3T3-L1 cells, knockdown of ROCK-II by RNA interference enhanced the expression of adipogenic transcription factors while that of ROCK-I did not. Moreover, Y-27632 inhibited IRS-1 serine phosphorylation and enhanced Akt phosphorylation in 3T3-L1 preadipocytes. Similarly, Akt phosphorylation in ROCK-II (−/−) MEFs was augmented compared with wild-type MEFs. In conclusion, inhibition of ROCK-II, not ROCK-I, enhances adipogenesis accompanied by the up-regulation of adipogenic transcription factors. Augmentation of insulin signaling may contribute to the enhancement of adipogenesis.

Adipogenesis is an area of intense interest because of the large and growing prevalence of obesity, insulin resistance, and type 2 diabetes (1, 2). Studies with *in vitro* models, such as 3T3-L1 and 3T3-F442A cell lines, have clarified the mechanisms of adipogenesis (3, 4). In 3T3-L1 cells, adipocyte differentiation is a process regulated by multiple transcription factors, principally the CCAAT/enhancer-binding protein (C/EBP)[2] family and peroxisome proliferator-activated receptor γ (PPARγ). In the presence of hormonal inducers, the expression of C/EBPβ and C/EBPδ temporarily increases (5), followed by the expression of PPARγ and C/EBPα (6, 7). A cooperative interaction between PPARγ and C/EBPα drives the expression of genes that are necessary for the generation and maintenance of the adipogenic phenotype such as lipid accumulation and insulin sensitivity (8).

During adipogenesis, adipocytes morphologically change from fibroblastic cells to round and lipid-laden cells. It is well known that actin cytoskeleton regulates the morphology of the cells (9). Concerning adipogenesis and actin cytoskeleton, it has been reported that adipocyte differentiation results in the conversion of filamentous actin (F-actin) from stress fibers and lamellipodia to cortical actin structures (10).

During the past several decades, many studies have shed light on the molecular mechanisms of actin cytoskeletal regulation. Members of the Rho family are essential regulatory components of the signaling pathway that directs reorganization of actin cytoskeleton. Small GTPase Rho contributes to many cellular functions such as cell motility, adhesion, and cytokinesis through reorganization of actin cytoskeleton. Rho is activated by extracellular signals such as lysophosphatidic acid (LPA). The actions of Rho are mediated by downstream Rho effectors. One of these effectors is Rho-associated kinase (ROCK) (11, 12). Two ROCK isoforms have been identified: ROCK-I (also known as ROKβ) and ROCK-II (also known as Rho kinase and ROKα) (13–16). ROCK mediates Rho signaling and reorganizes actin cytoskeleton through phosphorylation of several substrates that contribute to the assembly of actin filaments and contractility. Elucidation of the role of ROCK has been facilitated by the introduction of ROCK inhibitors, Y-27632 and fasudil. Studies with these inhibitors have revealed that ROCK

* This work was supported by research grants from the Japanese Ministry of Education, Culture, Sports, Science, and Technology and the Japanese Ministry of Health, Labor and Welfare. This work was also supported in part by a grant from the Smoking Research Foundation. The costs of publication of this article were defrayed in part by the payment of page charges. This article must therefore be hereby marked "*advertisement*" in accordance with 18 U.S.C. Section 1734 solely to indicate this fact.

[1] To whom correspondence should be addressed: Dept. of Medicine and Clinical Science, Kyoto University Graduate School of Medicine, 54 Shogoin Kawahara-cho, Sakyo-ku, Kyoto 606-8507, Japan. Tel.: 81-75-751-3172; Fax: 81-75-771-9452; E-mail: kh@kuhp.kyoto-u.ac.jp.

[2] The abbreviations used are: C/EBP, CCAAT/enhancer-binding protein; IRS, insulin receptor substrate; ERK, extracellular signal-related kinase; MAPK, mitogen-activated protein kinase; CS, calf serum; FBS, fetal bovine serum; DMEM, Dulbecco's modified Eagle medium; BSA, bovine serum albumin; PI3K, phosphatidylinositol 3-kinase; IGF-1, insulin-like growth factor-1; ROCK, Rho-associated kinase; PPARγ, proliferator-activated receptor γ; LPA, lysophosphatidic acid.

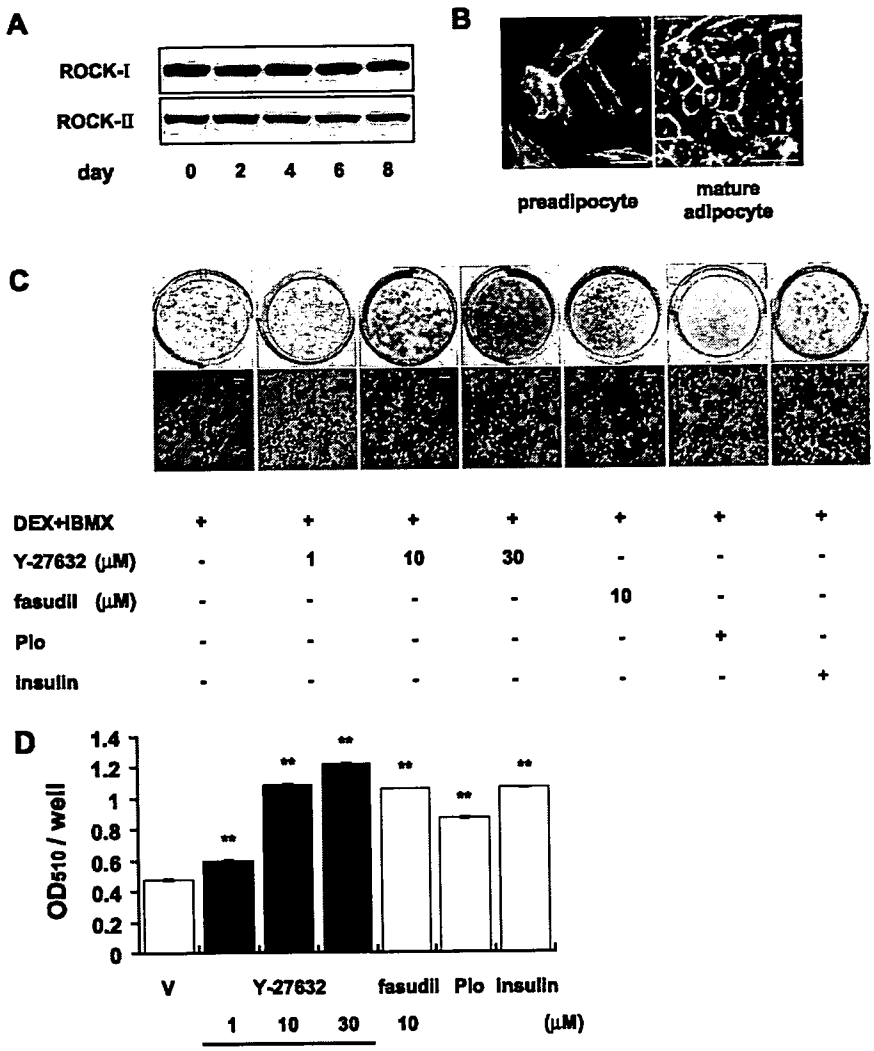

FIGURE 1. **ROCK expression and actin cytoskeleton during adipogenesis and effect of ROCK inhibitors on adipogenesis.** *A*, equal amounts of proteins harvested from day 0 to day 8 were subjected to Western blot analysis using antibodies against ROCK-I and ROCK-II. *B*, 3T3-L1 preadipocytes and mature adipocytes were fixed, permeabilized, and stained with Oregon Green phalloidin for F-actin. *Bar*, 50 μm. *C*, differentiated adipocytes were fixed and stained with Oil Red O at day 8. Macroscopic and microscopic pictures of cells are shown. *D*, lipid accumulation was assessed by the quantification of A_{510} in destained Oil Red O with isopropyl alcohol. Data are expressed as mean ± S.E. from triplicate experiments. **, $p < 0.01$ (Student's *t* test) compared with dexamethasone and IBMX-treated group. *Pio*, pioglitazone, *V*, vehicle.

regulates various physiological and pathological processes (17–20), while they cannot refer to the isoform-specific role of ROCK because ROCK inhibitors inhibit the activity of both ROCK-I and ROCK-II. Furthermore, ROCK inhibitors may potentially inhibit other protein kinases such as protein kinase A (12).

Several studies have reported that Rho-ROCK pathway is involved in adipogenesis (21, 22). However, the role of ROCK in adipogenesis still remains to be clarified. We show here the effects of inhibition of ROCK on adipogenesis and examine the molecular mechanisms using pharmacological and genetic approaches. Especially, the adipogenic analysis using MEFs derived from ROCK-I or ROCK-II knock-out mice and ROCK-I or ROCK-II siRNA can provide the evidence about the physiological role of ROCK and the isoform-specific role of ROCK in adipogenesis.

EXPERIMENTAL PROCEDURES

Materials—Y-27632 and pioglitazone (AD-4833) were provided by Mitsubishi Pharma (Osaka, Japan) and Takeda Pharmaceutical Company (Osaka, Japan), respectively. Insulin was purchased from Roche Applied Science (Mannheim, Germany). 3-Isobutyl-1-methylxanthine (IBMX) and dexamethasone were purchased from Nacalai Tesque, Inc. (Kyoto, Japan). LPA and wortmannin were obtained from Sigma-Aldrich (Tokyo, Japan). Fasudil was obtained from Calbiochem. Polyclonal antibodies against ROCK-I, ROCK-II, C/EBPα, C/EBPδ, PPARγ, and IRS-1 were purchased from Santa Cruz Biotechnology (Santa Cruz, CA). Monoclonal antibodies against C/EBPβ and adiponectin were obtained from Affinity BioReagents (Golden, CO). The monoclonal antibody against aP2 was purchased from R&D Systems (Minneapolis, MN). Polyclonal antibodies against Akt, phospho-Akt (Ser^{473}), phospho-IRS-1 ($Ser^{632/635}$), phospho-IRS-1 (Ser^{612}), ERK1/2, phospho-ERK1/2, p38MAPK, and phospho-p38MAPK were purchased from Cell Signaling Technology Inc. (Beverly, MA). Horseradish peroxidase-conjugated anti-mouse, anti-rat, and anti-rabbit IgG antibodies and ECL plus Western detecting kit were purchased from Amersham Biosciences.

Cell Culture, Adipocyte Differentiation, and Oil Red O Staining—3T3-L1 cells (kindly provided by Dr. H. Green and Dr. M. Morikawa, Harvard Medical School, Boston, MA) were cultured and differentiated into adipocytes as described previously (23). Briefly, cells were grown for 2 days post-confluence (referred as day 0) in 10% CS/DMEM. Differentiation was induced with 10% FBS/DMEM containing 0.5 mM IBMX, 0.25 μM dexamethasone, and 1 μg/ml insulin for 2 days. The cells were then incubated in 10% FBS/DMEM with insulin for 2 days and maintained hereafter with 10% FBS/DMEM to day 8. Pioglitazone was dissolved in Me_2SO and added to media within 0.1% of volume. The medium was changed every other day. At day 8, the cells were washed with phosphate-buffered saline (PBS) twice, fixed in 3.7% formaldehyde for 1 h and then stained with 0.6% (w/v) Oil Red O solution (60% isopropyl alcohol, 40% water) for 2 h at room temperature. Cells were then

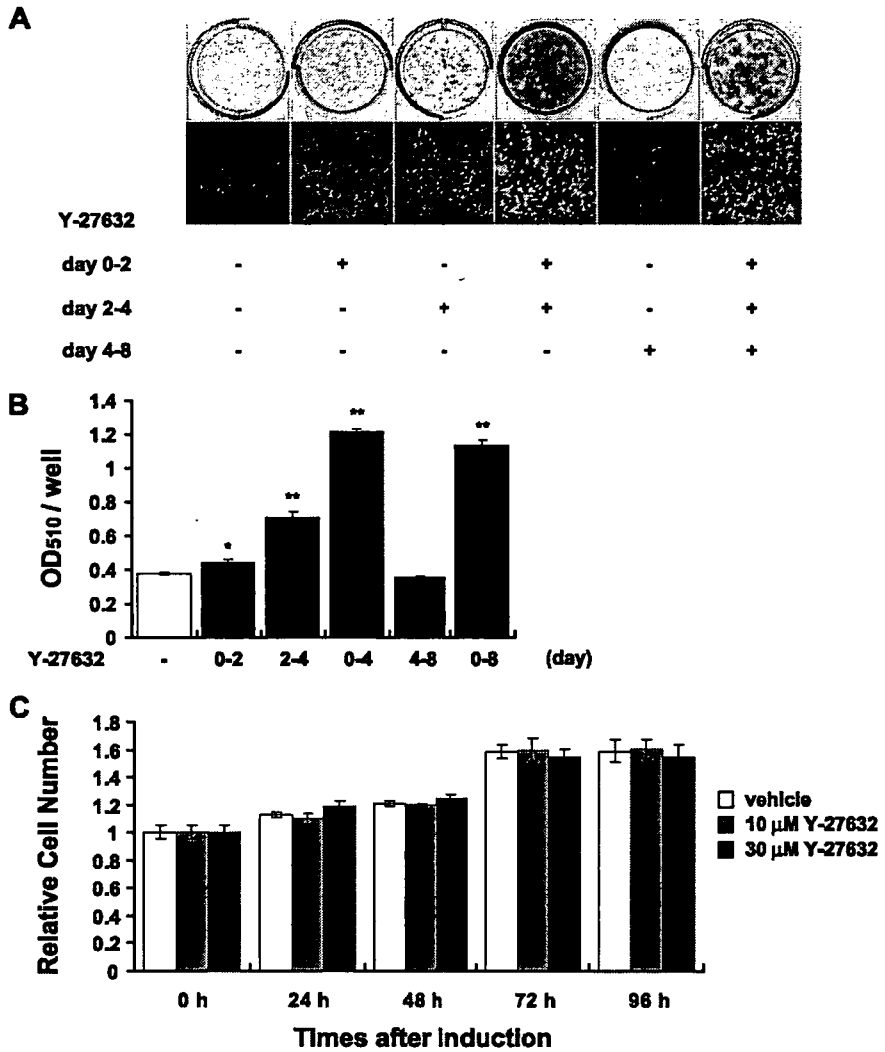

FIGURE 2. **Effect of Y-27632 during 3T3-L1 adipogenesis.** *A*, in the presence of dexamethasone and IBMX, 30 μM Y-27632 was supplemented from day 0 to day 2, day 2 to day 4, day 0 to day 4, day 4 to day 8 or day 0 to day 8, respectively. Differentiated adipocytes were fixed and stained with Oil Red O at day 8. Macroscopic and microscopic pictures of cells are shown. *B*, lipid accumulation was assessed by the quantification of A_{510} in destained Oil Red O with isopropyl alcohol. Data are expressed as mean ± S.E. from triplicate experiments. *, $p < 0.05$ (Student's *t* test) compared with dexamethasone and IBMX-treated group. **, $p < 0.01$ (Student's *t* test) compared with dexamethasone and IBMX-treated group. *C*, relative cell number during adipogenesis. 10 μM or 30 μM Y-27632 was added from day 0 to day 4 in the presence of dexamethasone and IBMX. Proliferation of MEFs was assessed by counting cells at the indicated times. Data are expressed as mean ± S.E. from triplicate experiments.

washed with water to remove unbound dye. Stained Oil Red O was eluted with isopropyl alcohol and quantified by measuring the optical absorbance at 510 nm (24).

Preparation of Primary Mouse Embryonic Fibroblasts and Induction of Adipogenesis—The generation of ROCK-I and ROCK-II knock-out mice was previously reported (25, 26). ROCK-II knock-out mice of a mixed background 129/Sv and C57BL/6N genetic background were backcrossed to the C57BL/6N strain for more than 8 generations. Primary MEFs were harvested from 13.5 d.p.c. embryos of each genotype as previously described (27). Differentiation of MEFs was induced with 0.5 mM IBMX, 0.25 μM dexamethasone and 10 μg/ml insulin for 6 days and maintained with 10% FBS/DMEM to day 8.

Small Interfering RNA (siRNA)—Synthetic siRNAs were purchased from Invitrogen (Carlsbad, CA). siRNAs were delivered into 3T3-L1 cells by a pulse of electroporation with Nucleofector (Amaxa, Gaithersburg, MD). After the electroporation, cells were immediately mixed with the fresh medium for 10 min and reseeded on plates for further examinations. The cells were differentiated 12 h after the electroporation. Negative control siRNA was used as the control of experiments. The targeted nucleotide sequences of the siRNAs were ATTGGTGCTTGTCAGTTAGGCGTGC (ROCK-I) and ATAATTACTCATAAGGTTGACGAGG (ROCK-II).

Preparation of Total Cell Lysates and Western Blot Analysis—Cells were washed twice with ice-cold PBS and harvested in a lysis buffer (40 mM HEPES, 10 mM EDTA, 100 mM NaF, 10 mM sodium pyrophosphate, 1 mM Na_3VO_4, 50 μM okadaic acid, 1% (v/v) Nonidet P-40, 1 mM phenylmethylsulfonyl fluoride, and 0.1 mg/ml aprotinin at pH 7.5). For the examination of transcription factors, cells were harvested in a lysis buffer (60 mM Tris-HCl and 1% SDS at pH 6.8). Lysates were heated at 100 °C for 10 min. After centrifugation, supernatants were normalized for protein concentration via the Bradford method and subjected to immunoblotting. For Western blot analysis, proteins were subjected to SDS-PAGE and electroblotted to polyvinylidene fluoride membranes (Polyscreen, NEN Life Science Products, Inc., Boston, MA). Transferred membranes were blocked with Block Ace (Yukijirushi Nyugyo, Sapporo, Japan) and then incubated with the primary antibodies. After washing with PBS, membranes were reacted with secondary antibodies and developed with ECL plus as instructed by the manufacturer. The signal on the blot was detected and quantified with Lumino-Image Analyser LAS-1000 System (Fuji Photo Film Co., Tokyo, Japan).

Immunofluorescence Study—The cells were washed once with PBS and fixed as follows. 3T3-L1 cells were fixed first for 1 min with 4% formaldehyde and 0.1% Triton X in PBS and then for 15 min with 4% formaldehyde alone in PBS. The cells were permeabilized by washing in PBS containing 0.1% Triton X for 5 min and incubated with PBS containing 3% bovine serum albumin for 60 min at room temperature. F-actin was stained with Oregon Green phalloidin (Molecular Probes, Carlsbad, CA). Optical sections were obtained with a Carl Zeiss LSM5 Pascal.

Quantitative Real-time PCR—Total RNA was prepared using TRIzol Reagent (Invitrogen). For quantitative RT-PCR assay, cDNA was synthesized by iScript (Bio-Rad). To determine ROCK-I, ROCK-II, PPARγ, and C/EBPα mRNA levels, these probes and primers were employed. ROCK-I-specific primers, sense: 5′-AGGAAAATACAGGAACTGCAAAGTG-3′, antisense: 5′-CTTTCTTGCTTTCCTGAGTCAACTC-3′ and probe: 5′-GTCTTCCAGAATCCCTCGCGCCAGCT-3′; ROCK-II-specific primers, sense: 5′-AAGACAGCGACATT-GAACAGC-3′, antisense: 5′-ACCATCCTTCTAATCTTGA-TTCTGG-3′ and probe: 5′-GATCCATCAGGCTCAGCATC-GCC-3′; PPARγ-specific primers, sense: 5′-CCCAGAGCAT-GGTGCCTT-3′, antisense: 5′-GGCATCTCTGTGTCAACC-ATGGT-3′ and probe: 5′-CTGATGCACTGCCTATGAGCA-CTTCACA-3′; C/EBPα-specific primers, sense: 5′-CGCCTT-CAACGACGAGTTC-3′, antisense: 5′-TTGGCCTTCTCCT-GCTGTC-3′, and probe: 5′-TGGCCGACCTCTTCCAGC-ACAG-3′. TaqMan PCR was performed using ABI Prism 7300 Sequence Detection System as instructed by manufacturer (Applied Biosystems, Foster City, CA). Levels of mRNA were normalized to those of 18S mRNA.

Statistical Analysis—Data are presented as means ± S.E. Student's *t* test was used to compare with the control. Differences were accepted as significant at $p < 0.05$ level.

RESULTS

ROCK Expression and Actin Cytoskeleton during Adipogenesis and Effect of ROCK Inhibitors on Adipogenesis—We detected protein expression of ROCK in 3T3-L1 cells by Western blot analysis (Fig. 1*A*). In 3T3-L1 preadipocytes (day 0) and mature adipocytes (day 8), both ROCK-I and ROCK-II were expressed. The expression levels of two ROCK isoforms did not significantly change during adipogenesis. Then, we observed actin cytoskeleton by phalloidin staining at preadipocytes and mature adipocytes. During adipogenesis, the structure of filamentous actin was converted from long stress fiber (preadipocyte) to cortical actin (mature adipocyte), suggesting that Rho-ROCK pathway is involved in adipogenesis (Fig. 1*B*). To examine the effects of ROCK inhibitors on adipogenesis, 3T3-L1 cells were exposed to 1 μM, 10 μM, 30 μM Y-27632, 10 μM fasudil, 1 μM pioglitazone, and 1 μg/ml insulin, respectively in the presence of dexamethasone and IBMX. Y-27632, fasudil, or pioglitazone was added to media from day 0 to day 8. Insulin was added to media from the start of differentiation (day 0) to day 4. At day 8, we evaluated the lipid accumulation by Oil Red O staining (Fig. 1, *C* and *D*). Y-27632 enhanced lipid accumulation in a dose-dependent manner. Y-27632 or fasudil-treated dishes accumulated lipid droplets markedly compared with vehicle-treated dishes, indicating that ROCK inhibitors enhance adipogenesis. Consistent with previous reports (28–30), insulin and pioglitazone enhanced lipid accumulation, respectively. Then, to determine when the ROCK inhibitor principally affects adipogenesis, 30 μM Y-27632 was added in various periods of 3T3-L1 adipogenesis stimulated by dexamethasone and IBMX (Fig. 2, *A* and *B*). The exposure of 30 μM Y-27632 during days 0–4 fully enhanced lipid accumulation, while during days 4–8, Y-27632 did not enhance it at all. In cases of days 0–2 and 2–4, Y-27632 partially enhanced lipid accumulation. Treatment with 10 μM or 30 μM Y-27632 did not significantly alter total cell number during adipogenesis compared with vehicle treatment (Fig. 2*C*).

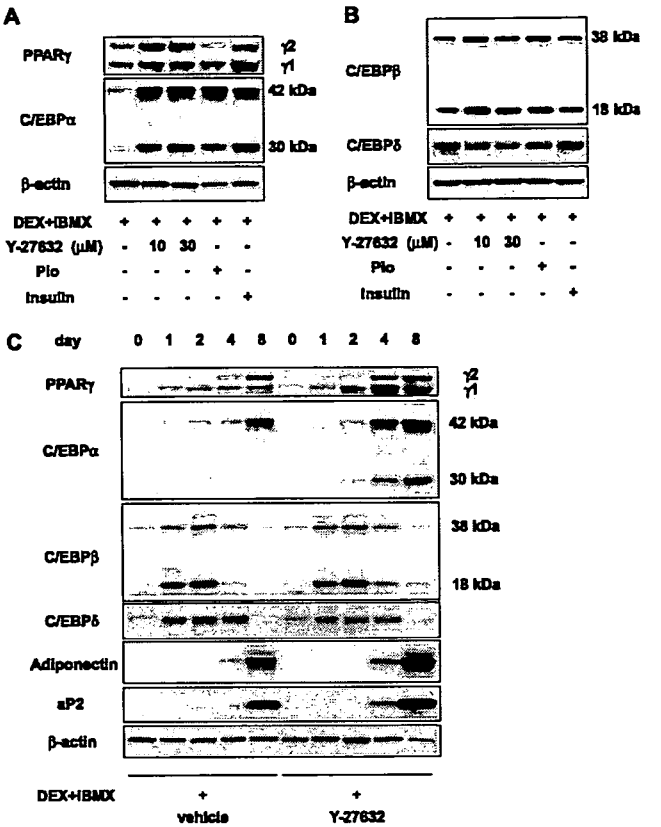

FIGURE 3. **Effect of Y-27632 on protein expression of adipogenic genes.** *A*, equal amounts of proteins harvested at day 4 were subjected to Western blot analysis using antibodies against PPARγ, C/EBPα, and β-actin. *B*, equal amounts of proteins harvested at day 2 were subjected to Western blot analysis using antibodies against C/EBPβ, C/EBPδ, and β-actin. *C*, equal amounts of proteins harvested at day 0, 1, 2, 4, and 8 were subjected to Western blot analysis using antibodies against PPARγ, C/EBPα, C/EBPβ, C/EBPδ, aP2, adiponectin, and β-actin. β-Actin proteins were monitored as hallmarks during adipocyte differentiation. *Pio*, pioglitazone. All data are representatives of at least three independent experiments.

Effect of Y-27632 on the Expression of Adipogenic Genes—Because ROCK inhibitors enhanced lipid accumulation, we examined the expression of adipogenic transcription factors C/EBPβ and C/EBPδ at day 2, and C/EBPα and PPARγ at day 4 by Western blot analysis (Fig. 3, *A* and *B*). In the presence of dexamethasone and IBMX, Y-27632 with a concentration of 30 μM augmented the expression of C/EBPβ (~1.8-fold increase), C/EBPα (~6.5-fold increase) and PPARγ (~5.6-fold increase) while it suppressed that of C/EBPδ (~40% decrease) compared with the non-treated group. 1 μg/ml insulin did not affect the expression of C/EBPβ and C/EBPδ at day 2 while it enhanced that of C/EBPα and PPARγ at day 4. 1 μM pioglitazone augmented the expression of C/EBPβ and C/EBPα while it suppressed those of C/EBPδ and PPARγ. The effects of insulin and pioglitazone on the expression of adipogenic trasnscription factors were compatible with previous reports (29, 31). Furthermore, we examined protein expression of adipogenic genes during the course of differentiation; day 0, day 1, day 2, day 4, and day 8 (Fig. 3*C*). Compared with the vehicle treatment

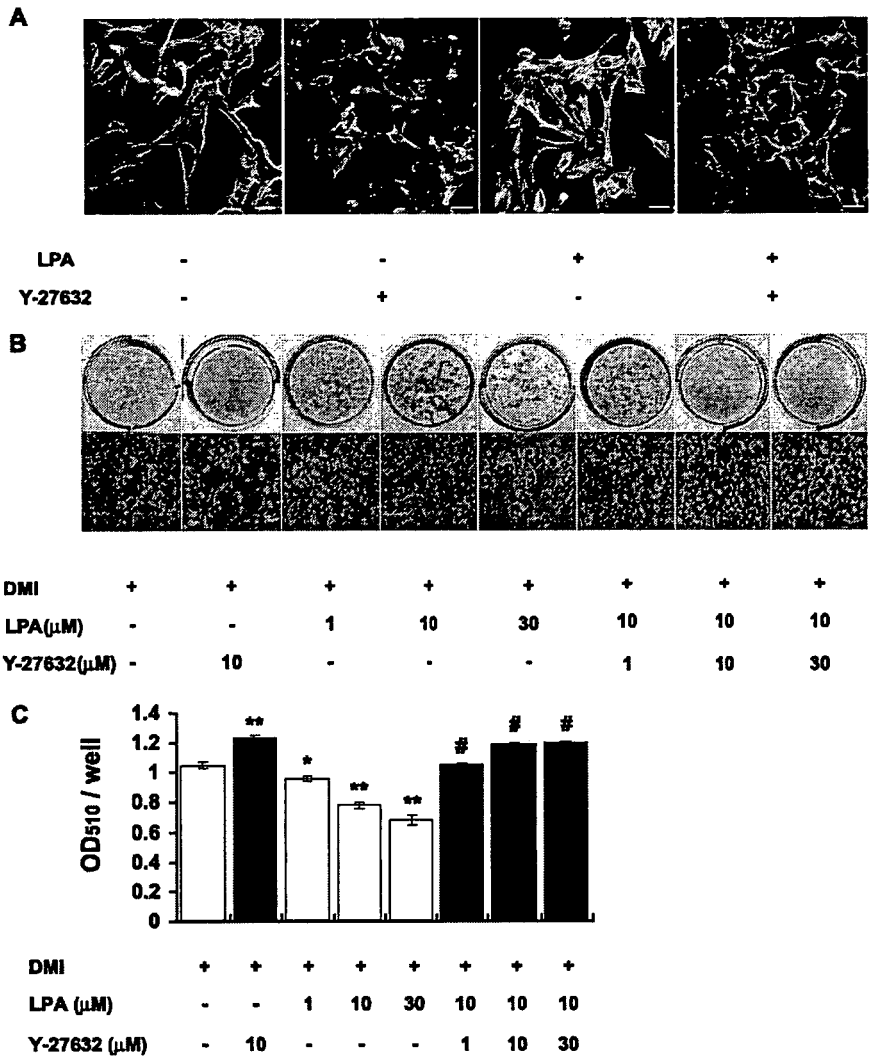

FIGURE 4. **Effect of LPA and Y-27632 on actin cytoskeleton and adipogenesis of 3T3-L1 preadipocytes.** *A*, 3T3-L1 cells were treated or not treated with 30 μM Y-27632 for 2 h, then exposed to 10 μM LPA for 0 and 5 min. The cells were fixed, permeabilized, and stained with Oregon Green phalloidin for F-actin. *Bar*, 50 μm. *B*, differentiated adipocytes were fixed and stained with Oil Red O at day 8. Macroscopic and microscopic pictures of cells are shown. *C*, lipid accumulation was assessed by the quantification of A_{510} in destained Oil Red O with isopropyl alcohol. Data are expressed as mean ± S.E. from triplicate experiments. *, $p < 0.05$ (Student's *t* test) compared with DMI-treated group. **, $p < 0.01$ (Student's *t* test) compared with DMI-treated group. #, $p < 0.01$ (Student's *t* test) compared with 10 μM LPA-treated group. DMI, dexamethasone, IBMX, and insulin.

group, 30 μM Y-27632 enhanced the expression of adipogenic transcription factors: C/EBPβ (~1.7-fold increase, day 1), PPARγ (~5.2-fold increase, day 4), and C/EBPα (~11.7-fold increase, day 4) and adipogenic late markers: aP2 (~8.9-fold increase, day 4) and adiponectin (~8.1-fold increase, day 4). Also in this analysis, Y-27632 suppressed the expression of C/EBPδ (~31% decrease, day 2).

Effect of LPA and Y-27632 on Actin Cytoskeleton and Adipogenesis—LPA activates small GTPase Rho via specific G protein-coupled receptors: LPA_{1-4} (32). It has been reported that LPA induces the stress fiber formation in Swiss 3T3 fibroblast, which is inhibited by Y-27632 (33, 34). Therefore, we examined the regulation of actin cytoskeleton by LPA and Y-27632 in 3T3-L1 preadipocytes (Fig. 4*A*). We stimulated serum-starved 3T3-L1 preadipocytes with or without 10 μM LPA after the pretreatment of 30 μM Y-27632 or non-treatment and assessed the effects on actin cytoskeleton by staining cells with phalloidin. LPA addition to serum-starved 3T3-L1 cells spread the cells and induced stress fibers while this change was inhibited by Y-27632. In Y-27632-treated cells without LPA addition, we could not observe stress fibers or thick actin rim in the cell periphery.

We examined the effects of Y-27632 on LPA-treated 3T3-L1 cells by Oil Red O staining. LPA and Y-27632 were added to media from day 0 to day 8. In the presence of dexamethasone, IBMX, and insulin, 10 μM Y-27632 enhanced adipogenesis (~20% increase) while 30 μM LPA inhibited it (~32% decrease), consistent with a previous report in 3T3-F442A cells (32). In 3T3-L1 cells, LPA inhibited adipogenesis in a dose-dependent manner with concentrations of 1 μM, 10 μM, and 30 μM. Y-27632 completely restored its inhibition with concentrations of 10 μM and 30 μM (Fig. 4, *B* and *C*).

Adipogenesis of ROCK-II (−/−) and ROCK-I (−/−) MEFs—To establish more directly causal link between ROCK and adipogenesis, primary mouse embryonic fibroblasts (MEFs) prepared from ROCK-II (+/+), ROCK-II (+/−), ROCK-II (−/−), and ROCK-I (+/+), ROCK-I (+/−), ROCK-I (−/−) mice were subjected to the adipogenic induction culture. Disruption of ROCK-I and ROCK-II protein was confirmed by Western blot analysis (Figs. 5*B* and 6*B*). ROCK-II protein levels in ROCK-I (+/+), ROCK-I (+/−), and ROCK-I (−/−) mice did not differ between genotypes. Similarly, ROCK-I protein levels in ROCK-II (+/+), (+/−), and (−/−) mice did not differ between genotypes. These results show that there is no compensatory increase in expression of the other ROCK isoform. After adipogenic induction, we examined lipid accumulation by Oil Red O staining and the expression of adipogenic transcription factors by Taqman PCR at day 8. ROCK-II (−/−) MEFs exhibited the enhancement of lipid accumulation compared with wild-type MEFs and mRNA levels of PPARγ and C/EBPα were markedly enhanced compared with wild-type MEFs (~14.2-fold and ~6.2-fold increase, respectively; **, $p < 0.01$). ROCK-II (+/−) MEFs also exhibited the enhancement of lipid accumulation compared with wild-type MEFs and mRNA levels of PPARγ and C/EBPα were significantly enhanced compared with wild-type MEFs (~5.4-fold and ~4.4-fold increase, respectively;

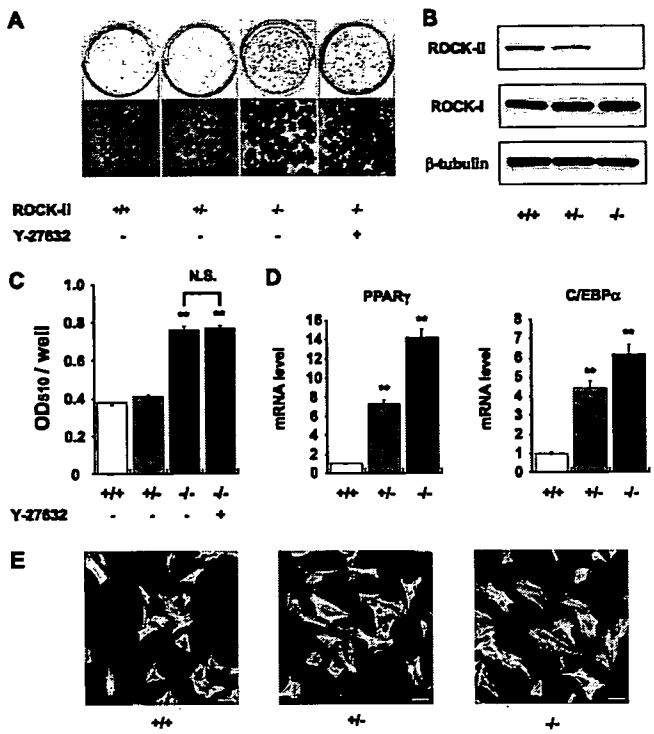

FIGURE 5. **Adipogenesis of ROCK-II (−/−) MEFs.** *A*, differentiated MEFs were fixed and stained with Oil Red O at day 8. Macroscopic and microscopic pictures of cells are shown. 30 μM Y-27632 was supplemented in the differentiation medium of ROCK-II (−/−) MEFs. *B*, equal amounts of proteins were subjected to Western blot analysis using antibodies against ROCK-I, ROCK-II, and β-tubulin. *C*, lipid accumulation was assessed by the quantification of A_{510} in destained Oil Red O with isopropyl alcohol. Data are expressed as mean ± S.E. from triplicate experiments. **, $p < 0.01$ (Student's *t* test) compared with ROCK-II (+/+) MEFs. *D*, expression of mRNA for PPARγ and C/EBPα from ROCK-II (+/+), (+/−) and (−/−) MEFs. Data are expressed as mean ± S.E. **, $p < 0.01$ (Student's *t* test) compared with ROCK-II (+/+) MEFs. $n = 6$ in each group. *E*, actin cytoskeleton of MEFs. Before adipogenic induction, the cells were fixed, permeabilized, and stained with Oregon Green phalloidin for F-actin. *Bar*, 50 μm.

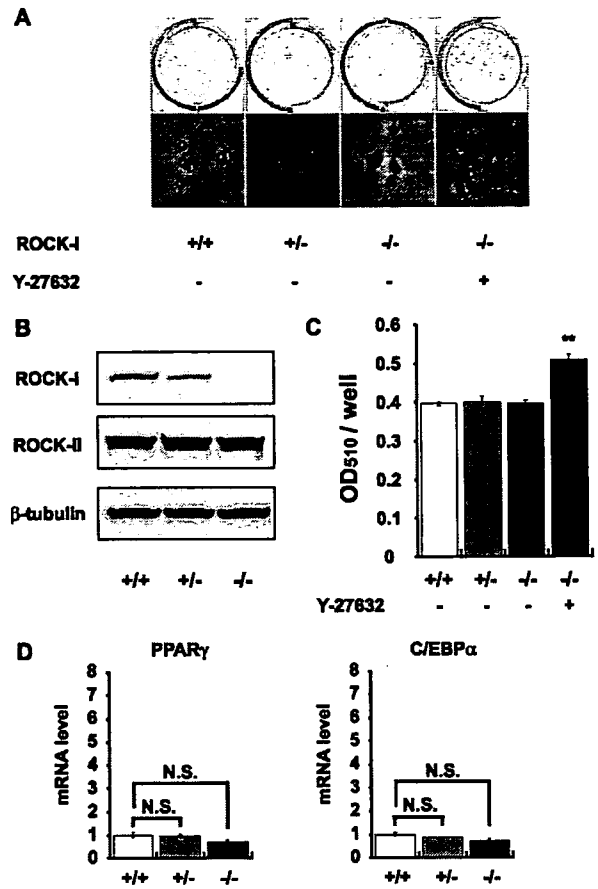

FIGURE 6. **Adipogenesis of ROCK-I (−/−) MEFs.** *A*, differentiated MEFs were fixed and stained with Oil Red O at day 8. Macroscopic and microscopic pictures of cells are shown. 30 μM Y-27632 was supplemented in the differentiation medium of ROCK-I (−/−) MEFs. *B*, equal amounts of proteins were subjected to Western blot analysis using antibodies against ROCK-I, ROCK-II, and β-tubulin. *C*, lipid accumulation was assessed by the quantification of A_{510} in destained Oil Red O with isopropyl alcohol. Data are expressed as mean ± S.E. from triplicate experiments. **, $p < 0.01$ (Student's *t* test) compared with ROCK-I (+/+) MEFs. *D*, expression of mRNA for PPARγ and C/EBPα from ROCK-I (+/+), (+/−), and (−/−) MEFs. Data are expressed as mean ± S.E. *N.S.*, not significant. $n = 6$ in each group.

**, $p < 0.01$). 30 μM Y-27632 did not enhance lipid accumulation in ROCK-II (−/−) MEFs, significantly (Fig. 5, *A*, *C*, and *D*). Before adipogenic induction, the architecture of actin cytoskeleton in ROCK-II (−/−) MEFs did not change compared with wild-type MEFs (Fig. 5*E*). The percentage of stress fiber positive cells was not significantly altered ((+/+), 96.67 ± 3.33%; (+/−), 97.22 ± 2.77%; (−/−), 97.1 ± 1.5%). In ROCK-I (−/−) MEFs, adipogenesis was not significantly enhanced compared with wild-type MEFs. Lipid accumulation and mRNA levels of PPARγ and C/EBPα did not differ between each genotype. Furthermore, 30 μM Y-27632 enhanced lipid accumulation in ROCK-I (−/−) MEFs (Fig. 6, *A*, *C*, and *D*).

Effect of Knockdown of ROCK on Expression of Adipogenic Transcription Factors—To determine whether inhibition of ROCK-II enhances adipogenesis in 3T3-L1 cells, we examined the effect of ROCK-I or ROCK-II knockdown on 3T3-L1 adipogenesis using siRNA technique. We introduced siRNA targeted for ROCK-I or ROCK-II into 3T3-L1 preadipocytes. 3T3-L1 cells were differentiated 12 h after introduction of siRNA. We confirmed the knockdown of ROCK-I or ROCK-II expression by Western blot analysis at day 2. Compared with the negative control group, introduction of ROCK-I and ROCK-II siRNA resulted in ~96 and ~86% decrease, respectively (Fig. 7, *A* and *B*). There was no obvious compensatory increase of the expression of the other ROCK isoform. At day 3, we examined the expression of adipogenic transcription factors by quantitative RT-PCR. ROCK-II siRNA enhanced the expression of PPARγ and C/EBPα compared with the control (~2.1-fold and ~1.8-fold increase, respectively, **, $p < 0.01$) (Fig. 7*C*). ROCK-I siRNA did not enhance the expression of PPARγ and C/EBPα significantly (Fig. 7*D*).

Effect of Inhibition of ROCK on Intracellular Signaling Pathway—We addressed the mechanisms of downstream signaling of Rho-ROCK. It is known that ROCK directly associates with IRS-1 and phosphorylates its serine residues (35–37). We stimulated serum-starved 3T3-L1 preadipocytes with insulin after the pretreatment of Y-27632. 30 μM Y-27632 inhibited insulin-induced IRS-1 Ser^{612} (~35% decrease, **, $p < 0.01$) and IRS-1 $Ser^{632/635}$ (~36% decrease, **, $p < 0.01$) phosphorylation and markedly enhanced insulin-induced Akt phosphorylation (~3.6-fold increase, **, $p < 0.01$) compared with non-treated

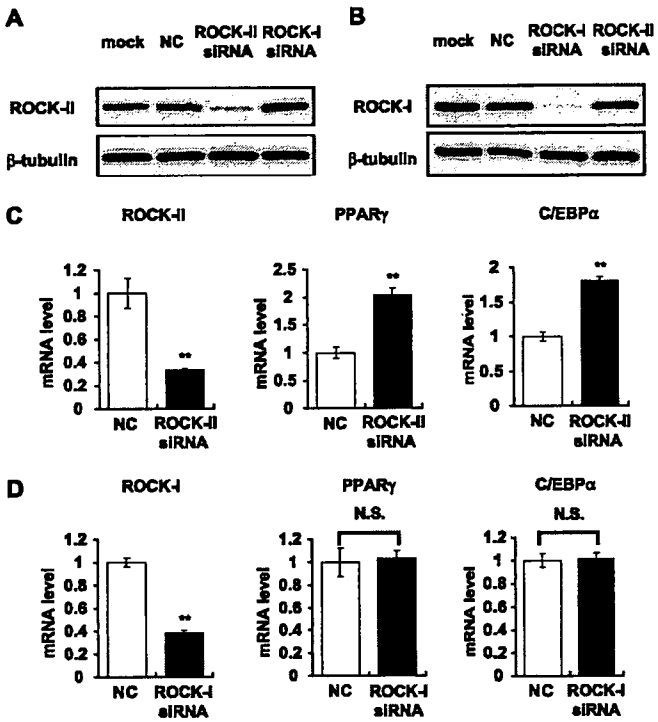

FIGURE 7. **Effect of knockdown of ROCK-I or ROCK-II on 3T3-L1 adipogenesis by RNA interference.** *A*, ROCK-II protein level was determined 48 h after adipogenic induction by Western blot analysis using antibodies against ROCK-II and β-tubulin. *B*, ROCK-I protein level was determined 48 h after adipogenic induction by Western blot analysis using antibodies against ROCK-I and β-tubulin. *C*, expression of mRNA for PPARγ, C/EBPα, and ROCK-II harvested at day 3. Data are expressed as mean ± S.E. **, $p < 0.01$ (Student's *t* test) compared with a negative control. $n = 6$ in each group. *D*, expression of mRNA for PPARγ, C/EBPα, and ROCK-I harvested at day 3. Data are expressed as mean ± S.E. *N.S.*, not significant. *NC*, negative control. $n = 6$ in each group.

groups (Fig. 8, *A* and *C*). Regarding MAPK signaling, Y-27632 slightly enhanced p38MAPK phosphorylation (~1.1-fold increase) and inhibited ERK1/2 phosphorylation (~23% decrease) upon the stimulation of insulin (Fig. 8*B*). We examined whether an inhibitor of PI3-kinase, wortmannin, blocks the enhancement of 3T3-L1 adipogenesis induced by Y-27632. Wortmannin and Y-27632 were added to media from day 0 to day 8. Wortmannin with concentrations of 100 nM and 1 μM inhibited the enhancement of preadipocyte differentiation induced by 10 μM Y-27632 in the presence of dexamethasone and IBMX (Fig. 8*D*). We examined insulin-induced Akt phosphorylation in ROCK-II knock-out MEFs. In ROCK-II (−/−) and (+/−) MEFs, insulin-induced Akt phosphorylation was significantly enhanced compared with wild-type MEFs (5 min after stimulation; ~6.0-fold increase and ~2.8-fold increase, respectively, **, $p < 0.01$) (Fig. 9*A*). In ROCK-I MEFs, there is no significant difference in insulin-induced Akt phosphorylation between each genotype (Fig. 9*B*).

DISCUSSION

In the present study, we show that inhibition of ROCK enhances adipogenesis. It is impossible to determine the isoform-specific role of ROCK by treatment of ROCK inhibitors. In addition to pharmacological approaches, we examined the adipogenesis of both ROCK-I (−/−) MEFs and ROCK-II (−/−) MEFs. Furthermore, we examined the effects of knockdown of ROCK-I or ROCK-II on 3T3-L1 adipogenesis by RNA interference. To the best of our knowledge, this is the first study demonstrating that inhibition of ROCK-II enhances adipogenesis and insulin-induced Akt phosphorylation. Our results suggest that ROCK-II plays an important role in adipogenesis and insulin signaling.

We examined the ROCK expression in 3T3-L1 cells by Western blot analysis. Both ROCK isoforms are expressed during the course of adipogenesis. A previous study showed that ROCK-II was expressed in 3T3-L1 mature adipocytes (36) while the expression of ROCK-I has not been reported.

Next, we examined the effects of ROCK inhibitors on lipid accumulation in 3T3-L1 cells. We found that two ROCK inhibitors, Y-27632 and fasudil, enhance lipid accumulation, respectively. These findings suggest that inhibition of ROCK enhances adipogenesis. We also assessed when Y-27632 affects adipogenesis. Supplementation with Y-27632 during days 0–4 fully enhances adipogenesis. These results let us speculate that inhibition of ROCK enhances the expression of adipogenic transcription factors. As expected, Y-27632 enhances the expression of adipogenic transcription factors, C/EBPβ, C/EBPα, and PPARγ in the presence of dexamethasone and IBMX, which indicates that inhibition of ROCK enhances adipogenesis through the up-regulation of adipogenic transcription factors. Following this, Y-27632 enhances the expression of adipogenic late markers, such as aP2 and adiponectin.

We assessed the effects of LPA and Y-27632 on adipogenesis and actin cytoskeleton. Because the Rho-ROCK pathway regulates actin cytoskeleton, we examined the effects of LPA and Y-27632 on actin cytoskeleton with phalloidin staining. We showed that stress fiber formation is augmented by LPA and that it is inhibited by Y-27632 in 3T3-L1 preadipocytes. These results provide the evidence that LPA activates the Rho-ROCK pathway and Y-27632 inhibits the pathway. Then, we showed that LPA inhibits adipogenesis in 3T3-L1 cells consistent with a previous report in 3T3-F442A cells. Furthermore, we showed that Y-27632 restores its inhibition in a dose-dependent manner. These results indicate that the Rho-ROCK pathway plays an important role in adipogenesis.

To determine the isoform-specific role of ROCK and to entirely exclude the nonspecific effects of ROCK inhibitors, we examined adipogenesis of ROCK-I (−/−) and ROCK-II (−/−) MEFs. We demonstrated that targeted disruption of ROCK-II enhances adipogenesis and that, in contrast, that of ROCK-I does not enhance adipogenesis. Furthermore, Y-27632 enhances lipid accumulation in ROCK-I (−/−) MEFs and does not enhance lipid accumulation in ROCK-II (−/−) MEFs. It suggests that inhibition of endogenous ROCK-II enhances adipogenesis. In 3T3-L1 cells, we examined the effect of knockdown of ROCK-I or ROCK-II on adipogenesis using siRNA. We showed that ROCK-II siRNA enhances the expression of adipogenic transcription factors while ROCK-I siRNA does not enhance it. Taken together, our results from the pharmacological and genetic approaches indicate that inhibition of ROCK, especially ROCK-II, enhances adipogenesis.

We investigated the mechanisms of the enhancement of adipogenesis by inhibition of ROCK. We demonstrated that Y-27632 inhibits IRS-1 serine phosphorylation and markedly

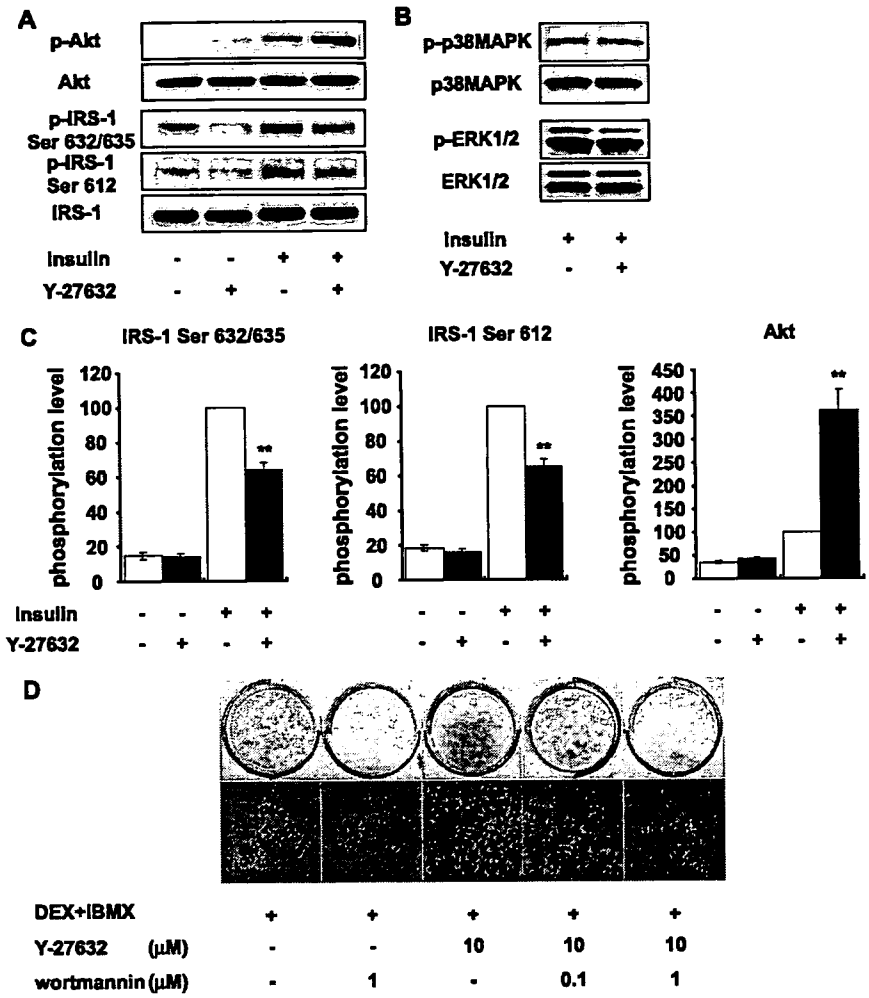

FIGURE 8. **Effect of inhibition of ROCK on intracellular signaling pathway in 3T3-L1 cells.** *A*, effect of Y-27632 on insulin signaling pathway. 3T3-L1 preadipocytes were stimulated with 10 nM insulin for 15 min or 100 nM insulin for 5 min in the absence or presence of 30 μM Y-27632. Western blot analysis was performed using antibodies against phospho-IRS-1 ($Ser^{632/635}$), phospho-IRS-1 (Ser^{612}), IRS-1, phospho-Akt (Ser^{473}), and Akt. All data are representatives of at least three independent experiments. *B*, effect of Y-27632 on MAPK signaling pathway. 3T3-L1 preadipocytes were stimulated with 100 nM insulin for 5 min in the absence or presence of 30 μM Y-27632. Western blot analysis was performed using antibodies against phospho-ERK1/2, ERK1/2, phospho-p38MAPK and p38MAPK. All data are representatives of at least three independent experiments. *C*, quantification of IRS-1 $Ser^{632/635}$ phosphorylation, IRS-1 Ser^{612} phosphorylation, and Akt phosphorylation. Phosphorylation level was normalized to total IRS-1 or total Akt level. Data are expressed as mean ± S.E. from triplicate experiments. **, $p < 0.01$ (Student's *t* test) compared with insulin-stimulated group without Y-27632. *Open bars* are treated without Y-27632. *D*, effect of wortmannin on the enhancement of 3T3-L1 adipogenesis induced by Y-27632. Differentiated adipocytes were fixed and stained with Oil Red O at day 8. Macroscopic and microscopic pictures of cells are shown.

enhances Akt phosphorylation upon the stimulation of insulin in 3T3-L1 preadipocytes. Previously, it has been reported that insulin/IGF-1 signaling is required for adipogenesis. MEFs derived from IRS-1 (−/−) mice do not have enough differentiation properties (27). IRS-1 and IRS-3 double knock-out mice exhibit lipodystrophy (38). Constitutively active Akt causes spontaneous differentiation in 3T3-L1 cells (39). Furthermore, we also demonstrated that an inhibitor of PI3-kinase, wortmannin, blocks the enhancement of adipogenesis induced by Y-27632. Therefore, augmentation of insulin signaling may contribute to the enhancement of preadipocyte differentiation. Concerning MAPK signaling, we showed that Y-27632 slightly enhances p38MAPK phosphorylation and slightly inhibits ERK1/2 phosphorylation in this cell line. Regarding ERK1/2 and p38MAPK, a great deal of evidence about the molecular link between MAPK and adipogenesis has been accumulating (40–45). However, their roles in adipogenesis are still controversial. In addition to pharmacological approaches, we showed that in ROCK-II (−/−) MEFs and even in ROCK-II (+/−) MEFs, insulin-induced Akt phosphorylation is enhanced compared with that in wild-type MEFs while in ROCK-I MEFs, there is no significant difference in insulin-induced Akt phosphorylation between each genotype. It provides the direct evidence that loss of ROCK-II enhances insulin-induced Akt phosphorylation.

Regarding the ROCK and insulin signaling, we showed that a ROCK inhibitor reduces IRS-1 serine phosphorylation and increases Akt phosphorylation in 3T3-L1 preadipocytes. It is known that ROCK directly associates with IRS-1 and phosphorylates its serine residues (35–37). In addition, previous studies have reported that IRS-1 serine phosphorylation negatively regulates insulin signaling in vascular smooth muscle cells (37) and NIH3T3 fibroblasts (46). However, recently, it has been reported that ROCK phosphorylates IRS-1 serine residues and positively regulates insulin signaling in 3T3-L1 mature adipocytes (36). The discrepancy between these reports shows that IRS-1 serine phosphorylation regulates insulin signaling differently depending on cell types. Therefore, there could be a difference in the regulation of insulin signaling by IRS-1 serine phosphorylation between preadipocytes and mature adipocytes.

Adipogenic analysis of both ROCK-I (−/−) and ROCK-II (−/−) MEFs revealed that loss of ROCK-II, not ROCK-I, enhances adipogenesis. The isoform-specific role of ROCK has been still obscure both *in vitro* and *in vivo*. As previously reported, loss of ROCK-I results in the eyelid open at birth (EOB) and omphalocele, while loss of ROCK-II results in placental dysfunction, intrauterine growth retardation, and fetal death. However, recently it has been reported that ROCK-II knock-out mice backcrossed in the C57BL6/N background exhibit not only the placental phenotype but also EOB and omphalocele (47). Concerning actin cytoskeletal regulation, it

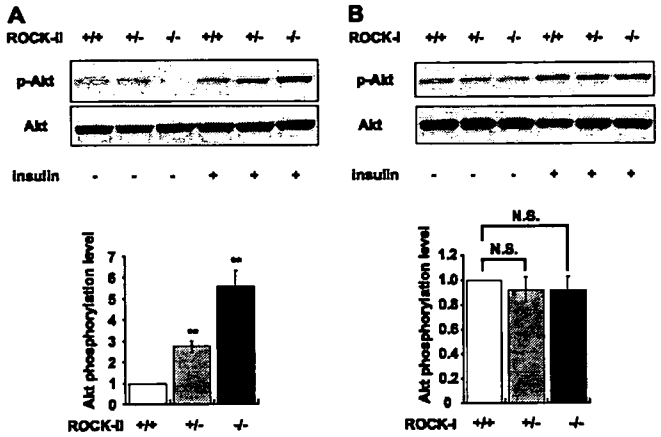

FIGURE 9. **Effect of knock-out of ROCK on insulin-induced Akt phosphorylation in MEFs.** *A*, insulin-induced Akt phosphorylation in ROCK-II (−/−) MEFs. ROCK-II (+/+), (+/−), and (−/−) MEFs were stimulated with 100 nM insulin for 5 min after serum starvation. Western blot analysis was performed using antibodies against phospho-Akt (Ser^{473}) and Akt. All data are representatives of at least three independent experiments. Quantification of insulin-induced Akt phosphorylation. Phospho-Akt level was normalized to total Akt level. Data are expressed as mean ± S.E. from triplicate experiments. **, $p < 0.01$ (Student's *t* test) compared with ROCK-II (+/+) MEFs. *B*, insulin-induced Akt phosphorylation in ROCK-I (−/−) MEFs. ROCK-I (+/+), (+/−), and (−/−) MEFs were stimulated with 100 nM insulin for 15 min after serum starvation. Western blot analysis was performed using antibodies against phospho-Akt (Ser^{473}) and Akt. All data are representatives of at least three independent experiments. Quantification of insulin-induced Akt phosphorylation. Phospho-Akt level was normalized to total Akt level. Data are expressed as mean ± S.E. from triplicate experiments. *N.S.*, not significant.

suggests that ROCK-I and ROCK-II cooperatively regulate actin bundle assembly required for eyelid and ventral body wall closure. In this context, our findings that inhibition of ROCK-II, not ROCK-I, enhances adipogenesis is a novel isoform-specific role of ROCK.

In summary, the present study first provides the robust and direct evidence that inhibition of ROCK-II enhances adipogenesis accompanied by the up-regulation of adipogenic transcription factors and that inhibition of ROCK-II enhances insulin-induced Akt phosphorylation. These results indicate that inhibition of ROCK-II enhances adipogenesis, at least in part, via augmentation of insulin signaling. Finally, these findings raise the possibility that ROCK-II is a novel target for the treatment of obesity, insulin resistance, and type 2 diabetes.

REFERENCES

1. Spiegelman, B. M., and Flier, J. S. (2001) *Cell* **104,** 531–543
2. Flier, J. S. (2004) *Cell* **116,** 337–350
3. Hwang, C. S., Loftus, T. M., Mandrup, S., and Lane, M. D. (1997) *Annu. Rev. Cell Dev. Biol.* **13,** 231–259
4. Rosen, E. D., and Spiegelman, B. M. (2000) *Annu. Rev. Cell Dev. Biol.* **16,** 145–171
5. Cao, Z., Umek, R. M., and McKnight, S. L. (1991) *Genes Dev.* **5,** 1538–1552
6. Tontonoz, P., Hu, E., Graves, R. A., Budavari, A. I., and Spiegelman, B. M. (1994) *Genes Dev.* **8,** 1224–1234
7. Lane, M. D., Tang, Q. Q., and Jiang, M. S. (1999) *Biochem. Biophys. Res. Commun.* **266,** 677–683
8. Wu, Z., Rosen, E. D., Brun, R., Hauser, S., Adelmant, G., Troy, A. E., McKeon, C., Darlington, G. J., and Spiegelman, B. M. (1999) *Mol. Cell* **3,** 151–158
9. Jaffe, A. B., and Hall, A. (2005) *Annu. Rev. Cell Dev. Biol.* **21,** 247–269
10. Kanzaki, M., and Pessin, J. E. (2001) *J. Biol. Chem.* **276,** 42436–42444
11. Etienne-Manneville, S., and Hall, A. (2002) *Nature* **420,** 629–635
12. Riento, K., and Ridley, A. J. (2003) *Nat. Rev. Mol. Cell Biol.* **4,** 446–456
13. Leung, T., Chen, X. Q., Manser, E., and Lim, L. (1996) *Mol. Cell. Biol.* **16,** 5313–5327
14. Leung, T., Manser, E., Tan, L., and Lim, L. (1995) *J. Biol. Chem.* **270,** 29051–29054
15. Ishizaki, T., Maekawa, M., Fujisawa, K., Okawa, K., Iwamatsu, A., Fujita, A., Watanabe, N., Saito, Y., Kakizuka, A., Morii, N., and Narumiya, S. (1996) *EMBO J.* **15,** 1885–1893
16. Matsui, T., Amano, M., Yamamoto, T., Chihara, K., Nakafuku, M., Ito, M., Nakano, T., Okawa, K., Iwamatsu, A., and Kaibuchi, K. (1996) *EMBO J.* **15,** 2208–2216
17. Uehata, M., Ishizaki, T., Satoh, H., Ono, T., Kawahara, T., Morishita, T., Tamakawa, H., Yamagami, K., Inui, J., Maekawa, M., and Narumiya, S. (1997) *Nature* **389,** 990–994
18. Itoh, K., Yoshioka, K., Akedo, H., Uehata, M., Ishizaki, T., and Narumiya, S. (1999) *Nat. Med.* **5,** 221–225
19. Shimokawa, H., Seto, M., Katsumata, N., Amano, M., Kozai, T., Yamawaki, T., Kuwata, K., Kandabashi, T., Egashira, K., Ikegaki, I., Asano, T., Kaibuchi, K., and Takeshita, A. (1999) *Cardiovasc. Res.* **43,** 1029–1039
20. Sawada, N., Itoh, H., Ueyama, K., Yamashita, J., Doi, K., Chun, T. H., Inoue, M., Masatsugu, K., Saito, T., Fukunaga, Y., Sakaguchi, S., Arai, H., Ohno, N., Komeda, M., and Nakao, K. (2000) *Circulation* **101,** 2030–2033
21. Sordella, R., Jiang, W., Chen, G. C., Curto, M., and Settleman, J. (2003) *Cell* **113,** 147–158
22. McBeath, R., Pirone, D. M., Nelson, C. M., Bhadriraju, K., and Chen, C. S. (2004) *Dev. Cell* **6,** 483–495
23. Frost, S. C., and Lane, M. D. (1985) *J. Biol. Chem.* **260,** 2646–2652
24. Ramirez-Zacarias, J. L., Castro-Munozledo, F., and Kuri-Harcuch, W. (1992) *Histochemistry* **97,** 493–497
25. Shimizu, Y., Thumkeo, D., Keel, J., Ishizaki, T., Oshima, H., Oshima, M., Noda, Y., Matsumura, F., Taketo, M. M., and Narumiya, S. (2005) *J. Cell Biol.* **168,** 941–953
26. Thumkeo, D., Keel, J., Ishizaki, T., Hirose, M., Nonomura, K., Oshima, H., Oshima, M., Taketo, M. M., and Narumiya, S. (2003) *Mol. Cell. Biol.* **23,** 5043–5055
27. Miki, H., Yamauchi, T., Suzuki, R., Komeda, K., Tsuchida, A., Kubota, N., Terauchi, Y., Kamon, J., Kaburagi, Y., Matsui, J., Akanuma, Y., Nagai, R., Kimura, S., Tobe, K., and Kadowaki, T. (2001) *Mol. Cell. Biol.* **21,** 2521–2532
28. Sandouk, T., Reda, D., and Hofmann, C. (1993) *Am. J. Physiol.* **264,** C1600–C1608
29. Norisada, N., Masuzaki, H., Fujimoto, M., Inoue, G., Hosoda, K., Hayashi, T., Watanabe, M., Muraoka, S., Yoneda, F., and Nakao, K. (2004) *Metabolism* **53,** 1532–1537
30. Kletzien, R. F., Clarke, S. D., and Ulrich, R. G. (1992) *Mol. Pharmacol.* **41,** 393–398
31. Rosen, E. D., Walkey, C. J., Puigserver, P., and Spiegelman, B. M. (2000) *Genes Dev.* **14,** 1293–1307
32. Simon, M. F., Daviaud, D., Pradere, J. P., Gres, S., Guigne, C., Wabitsch, M., Chun, J., Valet, P., and Saulnier-Blache, J. S. (2005) *J. Biol. Chem.* **280,** 14656–14662
33. Tsuji, T., Ishizaki, T., Okamoto, M., Higashida, C., Kimura, K., Furuyashiki, T., Arakawa, Y., Birge, R. B., Nakamoto, T., Hirai, H., and Narumiya, S. (2002) *J. Cell Biol.* **157,** 819–830
34. Ridley, A. J., and Hall, A. (1992) *Cell* **70,** 389–399
35. Farah, S., Agazie, Y., Ohan, N., Ngsee, J. K., and Liu, X. J. (1998) *J. Biol. Chem.* **273,** 4740–4746
36. Furukawa, N., Ongusaha, P., Jahng, W. J., Araki, K., Choi, C. S., Kim, H. J., Lee, Y. H., Kaibuchi, K., Kahn, B. B., Masuzaki, H., Kim, J. K., Lee, S. W., and Kim, Y. B. (2005) *Cell Metab.* **2,** 119–129
37. Begum, N., Sandu, O. A., Ito, M., Lohmann, S. M., and Smolenski, A. (2002) *J. Biol. Chem.* **277,** 6214–6222
38. Laustsen, P. G., Michael, M. D., Crute, B. E., Cohen, S. E., Ueki, K., Kulkarni, R. N., Keller, S. R., Lienhard, G. E., and Kahn, C. R. (2002) *Genes Dev.* **16,** 3213–3222
39. Kohn, A. D., Summers, S. A., Birnbaum, M. J., and Roth, R. A. (1996) *J. Biol. Chem.* **271,** 31372–31378

40. Belmonte, N., Phillips, B. W., Massiera, F., Villageois, P., Wdziekonski, B., Saint-Marc, P., Nichols, J., Aubert, J., Saeki, K., Yuo, A., Narumiya, S., Ailhaud, G., and Dani, C. (2001) *Mol. Endocrinol.* **15**, 2037–2049
41. Benito, M., Porras, A., Nebreda, A. R., and Santos, E. (1991) *Science* **253**, 565–568
42. Camp, H. S., and Tafuri, S. R. (1997) *J. Biol. Chem.* **272**, 10811–10816
43. Engelman, J. A., Lisanti, M. P., and Scherer, P. E. (1998) *J. Biol. Chem.* **273**, 32111–32120
44. Hu, E., Kim, J. B., Sarraf, P., and Spiegelman, B. M. (1996) *Science* **274**, 2100–2103
45. Prusty, D., Park, B. H., Davis, K. E., and Farmer, S. R. (2002) *J. Biol. Chem.* **277**, 46226–46232
46. Ozes, O. N., Akca, H., Mayo, L. D., Gustin, J. A., Maehama, T., Dixon, J. E., and Donner, D. B. (2001) *Proc. Natl. Acad. Sci. U. S. A.* **98**, 4640–4645
47. Thumkeo, D., Shimizu, Y., Sakamoto, S., Yamada, S., and Narumiya, S. (2005) *Genes Cells* **10**, 825–834

0013-7227/07/$15.00/0
Printed in U.S.A.

Endocrinology 148(11):5268–5277

doi: 10.1210/en.2007-0349

Ceramide and Adenosine 5′-Monophosphate-Activated Protein Kinase Are Two Novel Regulators of 11β-Hydroxysteroid Dehydrogenase Type 1 Expression and Activity in Cultured Preadipocytes

N. Arai, H. Masuzaki, T. Tanaka, T. Ishii, S. Yasue, N. Kobayashi, T. Tomita, M. Noguchi, T. Kusakabe, J. Fujikura, K. Ebihara, M. Hirata, K. Hosoda, T. Hayashi, H. Sawai, Y. Minokoshi, and K. Nakao

Division of Endocrinology and Metabolism (N.A., H.M., T.Ta., T.I., S.Y., N.K., T.To., M.N., T.K., J.F., K.E., M.H., K.H., K.N.), Department of Medicine and Clinical Science, Kyoto University Graduate School of Medicine, Kyoto 606-8507, Japan; Department of Human Coexistence (T.H.), Kyoto University Graduate School of Human and Environmental Studies, Kyoto 606-8501, Japan; Department of Internal Medicine (H.S.), Osaka Dental University, Osaka 573-1121, Japan; and Department of Developmental Physiology (Y.M.), National Institute for Physiological Science, Aichi 444-8585, Japan

Increased activity of intracellular glucocorticoid reactivating enzyme, 11β-hydroxysteroid dehydrogenase type 1 (11β-HSD1) in obese adipose tissue contributes to adipose dysfunction. As recent studies have highlighted a potential role of preadipocytes in adipose dysfunction, we tested the hypothesis that a variety of metabolic stress mediated by ceramide or AMP-activated protein kinase (AMPK) would regulate 11β-HSD1 in preadipocytes. The present study is the first to show that 1) expression of 11β-HSD1 in 3T3-L1 preadipocytes was robustly induced when cells were treated with cell-permeable ceramide analogue C_2 ceramide, bacterial sphingomyelinase, and sphingosine 1-phosphate, 2) 5-aminoimidazole-4-carboxamide ribonucleoside (AICAR)-induced activation of AMPK augmented the expression and enzyme activity of 11β-HSD1, and 3) these results were reproduced in human preadipocytes. We demonstrate for the first time that C_2 ceramide and AICAR markedly induced the expression of CCAAT/enhancer-binding protein (C/EBP) β and its binding to 11β-HSD1 promoter. Transient knockdown of C/EBPβ protein by small interfering RNA markedly attenuated the expression of 11β-HSD1 induced by C_2 ceramide or AICAR. The present study provides novel evidence that ceramide- and AMPK-mediated signaling pathways augment the expression and activity of 11β-HSD1 in preadipocytes by way of C/EBPβ, thereby highlighting a novel, metabolic stress-related regulation of 11β-HSD1 in a cell-specific manner. (*Endocrinology* 148: 5268–5277, 2007)

METABOLIC SYNDROME IS characterized by a cluster of glucose intolerance, hypertension, and dyslipidemia on a basis of insulin resistance and excess in intraabdominal fat accumulation (1–3). Functional abnormalities of adipose tissue have been implicated in the pathophysiology of metabolic syndrome (2). A series of transgenic and knockout experiments in mouse models suggest that exaggerated reactivation of glucocorticoid in adipose tissue, mediated by enzyme 11β-hydroxysteroid dehydrogenase type 1 (11β-HSD1), contributes to dysfunction of adipose tissue (3–7). 11β-HSD1 is a bidirectional (oxo-reductase and dehydrogenase) enzyme (8), expressing abundantly in adipose tissue, liver, and central nervous system (9, 10). Notably, 11β-HSD1 mainly acts as an oxo-reductase *in vivo* and reactivates inactive cortisone into active cortisol (8). Transgenic mice overexpressing 11β-HSD1 in adipose tissue exemplified major phenotype of metabolic syndrome (3, 4), whereas systemic 11β-HSD1 knockout mice were protected against diabetes and dyslipidemia on a high-fat diet (5–7). These data suggest that an increased level of adipose 11β-HSD1 considerably contributes to metabolic derangement. Consistent with this notion, selective 11β-HSD1 inhibitors are shown to ameliorate diabetes, dyslipidemia, and arteriosclerosis in experimental murine models (11, 12).

Obese adipose tissue is subjected to multiple cellular stresses such as endoplasmic reticulum stress and oxidative stress (13). Local hypoxia, tissue dysnutrition, and resultant cell death are potentially linked to macrophage recruitment and local inflammation in adipose tissue (13, 14). Recent studies also highlight a complexity of preadipocytes in controlling adipose tissue function (15, 16). Nevertheless mature adipocytes are the major component of adipose tissue and predominant source of 11β-HSD1 (10, 17); a considerable amount of 11β-HSD1 expression is also detected in stromal-vascular cells from adipose tissue (17). The underlying mechanism whereby 11β-HSD1 is elevated in obese adipose tissue still remains obscure, and the regulation of 11β-HSD1 in preadipocytes has been poorly understood.

In this context, we hypothesized that a variety of metabolic stresses would regulate the expression of 11β-HSD1 in preadipocytes. The sphingolipid ceramide serves as a bioactive lipid mediator in response to a variety of metabolic stresses

First Published Online August 16, 2007

Abbreviations: ACC, Acetyl-CoA carboxylase; AICAR, 5-aminoimidazole-4-carboxamide ribonucleosides; AMPK, AMP-activated protein kinase; C/EBP, CCAAT/enhancer-binding protein; ChIP, chromatin immunoprecipitation; 11β-HSD1, 11β-hydroxysteroid dehydronenase type 1; MCP-1, monocyte chemoattractant protein-1; Pref-1, preadipocyte factor-1; SMase, sphingomyelinase; S1P, sphingosine 1-phosphate; siRNA, small interfering RNA.

Endocrinology is published monthly by The Endocrine Society (http://www.endo-society.org), the foremost professional society serving the endocrine community.